FRACTIONAL QUANTUM ENERGY LEVELS OF HYDROGEN

ELECTROLYTIC DEVICES

KEYWORDS: *X-ray photoelectron spectroscopy, lower energy hydrogen, mass spectroscopy*

RANDELL L. MILLS and WILLIAM R. GOOD
HydroCatalysis Power Corporation, Great Valley Corporate Center
41 Great Valley Parkway, Malvern, Pennsylvania 19355

Received May 23, 1994
Accepted for Publication December 19, 1994

Report is made of the detection of atomic hydrogen in fractional quantum energy levels below the traditional "ground" state—hydrinos—by X-ray photoelectron spectroscopy and by a reinterpretation of soft X-ray emissions from the interstellar medium. Hydrino formation occurs with the release of energy on nickel cathodes during the electrolysis of aqueous potassium carbonate. The detection of a new molecular species—the diatomic hydrino molecule—by high-resolution mass spectroscopy is also reported.

I. INTRODUCTION

J. J. Balmer showed, in 1885, that the frequencies for some of the lines observed in the emission spectrum of atomic hydrogen could be expressed with a completely empirical relationship. This approach was later extended by J. R. Rydberg, who showed that all of the spectral lines of atomic hydrogen were given by the equation

$$\bar{\nu} = R\left(\frac{1}{n_f^2} - \frac{1}{n_i^2}\right) , \qquad (1)$$

where $R = 109\,677\ \text{cm}^{-1}$, $n_f = 1, 2, 3, \ldots$, $n_i = 2, 3, 4, \ldots$, and $n_i > n_f$.

Niels Bohr, in 1913, developed a theory for atomic hydrogen that gave energy levels in agreement with Rydberg's equation. An identical equation, based on a totally different theory for the hydrogen atom, was developed by E. Schrödinger, and independently by W. Heisenberg, in 1926:

$$E_n = -\frac{e^2}{n^2 8\pi\epsilon_0 a_H} = -\frac{13.598\ \text{eV}}{n^2} \qquad (2a)$$

$$n = 1,2,3,\ldots , \qquad (2b)$$

where a_H is the Bohr radius for the hydrogen atom, 52.947 pm, e is the magnitude of the charge of the electron, and ϵ_0 is the vacuum permittivity.

The purpose of this paper is to describe a number of experimental observations that lead to the conclusion that atomic hydrogen can exist in fractional quantum states that are at lower energies than the traditional "ground" ($n = 1$) state. Explicitly, we propose that the energy-level equation for atomic hydrogen is as given in Eq. (2a), but the restriction on "n," Eq. (2b), should be replaced by Eq. (2c):

$$n = 1,2,3,\ldots , \quad \text{and} \quad n = \tfrac{1}{2},\tfrac{1}{3},\tfrac{1}{4},\ldots . \qquad (2c)$$

The complete theory is given elsewhere.[1,2] The central feature of this theory is that all particles (atomic-size particles and macroscopic particles) obey the same physical laws. Whereas Schrödinger postulated a boundary condition: $\Psi \to 0$ as $r \to \infty$, which leads to a purely mathematical model of the electron, the boundary condition in this theory was derived from Maxwell's equations[3]:

> *For non-radiative states, the current-density function must not possess space-time Fourier components that are synchronous with waves traveling at the speed of light.*

Application of the latter boundary condition leads to an entirely different model of particles, atoms, molecules, and to a very different concept of the nature of the physical universe.[1,2]

This paper has been organized as follows: Sec. II describes the determination of excess heat release during the electrolysis of aqueous potassium carbonate and how a catalytic reaction of atomic hydrogen from $n = 1$ to fractional quantum energy levels accounts for this excess heat. Section III describes the experimental identification of hydrogen atoms in fractional quantum energy levels—hydrinos—by X-ray photoelectron spectroscopy (XPS) of the electrodes from these electrolytic cells. Section IV describes the experimental identification of hydrinos by emissions of soft X rays from

the dark interstellar medium. Section V describes the experimental identification of hydrogen molecules in fractional quantum energy levels—dihydrino molecules—by high-resolution magnetic sector mass spectroscopy. Section VI gives a summary.

II. EXCESS HEAT RELEASE DURING THE ELECTROLYSIS OF AQUEOUS POTASSIUM CARBONATE

II.A. Calorimetry Methods

Pulsed-current electrolysis of aqueous potassium carbonate at a nickel cathode was performed in a single-cell calorimeter. The cell operated at 50°C and was designed to have primarily conductive and convective heat losses to a water-cooled condenser. The output power was determined by flow calorimetry of the condenser coolant and the input power was measured with a power meter.

The calorimeter/electrolysis cell, Fig. 1, was a 16.5-ℓ vacuum-jacketed dewar[a] with a 4-in. inside diameter (i.d.) opening. A 60-in.-long × 3.9-in. outside diameter (o.d.) glass test tube liner (11.5 ℓ) was placed in the 79.75-in.-long dewar. This inner glass tube liner held the cathode, the anode, and the electrolyte. The calorimeter was sealed with a 3-in.-thick machined Teflon cap with two outer-diameter Vitron O-rings. The cap had perforations fitted with glass sleeves having inner-diameter Vitron O-ring seals[b] for the electrode leads and the condenser. The Graham condenser was a 10-mm-i.d. glass spiral, 35 cm in length, which was sealed in a 5-cm diam cylindrical water jacket.[c] Tygon tubing connected the inlet of the condenser to a peristaltic pump, the outlet of the condenser to a 5-gal reservoir, and the reservoir to the pump inlet. The water coolant reservoir was maintained at ambient temperature by a constant temperature chiller.[d] The condenser-water flow rate (±0.1 ml/min) was measured from the digital readout of the peristaltic pump[e] and confirmed with a stopwatch and volumetric measurements. The condenser-water inlet temperature (±0.1°C) and outlet temperature (±0.1°C) were each recorded with a microprocessor thermometer[f] using a type K thermocouple, which was inserted into the inlet or outlet of the condenser. The temperature (±0.1°C) of the electrolyte was measured with a microprocessor thermometer[f] using a type K thermocouple inserted through the Teflon cap. The resistance heater used during the calibration of the efficiency of heat transfer to the condenser was a 120 V/600 W Incoloy-alloy-coated[g] hermetically sealed heater.[h] The power was supplied by a constant power (±0.1%) supply.[i] The voltage (±0.1%) and current (±0.1%) were recorded with a digital multimeter.[j]

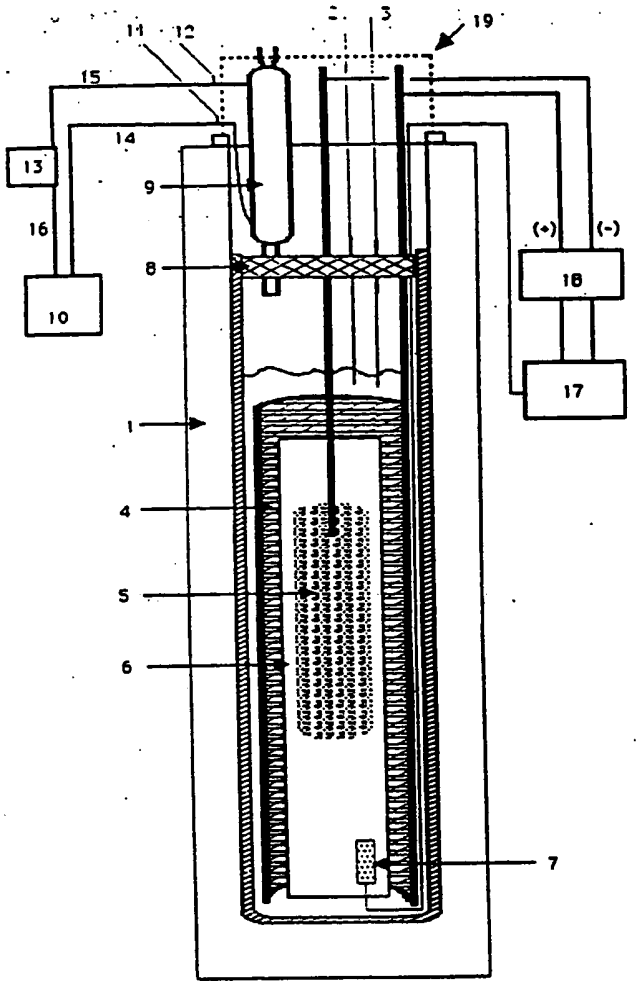

Fig. 1. The calorimeter/electrolysis cell: 1 = vacuum jacketed dewar, 2 = electrolyte thermistor, 3 = conductivity sensor, 4 = nickel anode, 5 = nickel cathode, 6 = Teflon spacer, 7 = resistor heater, 8 = Teflon cap, 9 = condenser, 10 = peristaltic pump, 11 = inlet thermistor, 12 = outlet thermistor, 13 = water reservoir, 14 = condenser inlet tubing, 15 = condenser outlet tubing, 16 = reservoir to pump tubing, 17 = power supply, function generator, power meter, 18 = oscilloscope, 19 = insulated cap.

The general form of the energy balance equation for the cell in steady state is

$$0 = P_{in} + P_{xs} - P_{loss} \ , \qquad (3)$$

[a]International Cryonics, Inc.
[b]Ace Glass 7644.
[c]At-Mar Glass.
[d]Yamato-Komatsu Coolnics Circulator CTE 24A.
[e]Masterflex Microprocessor Pump Drive, model 7524-00.
[f]Omega HH21.
[g]INCOLOY is a trademark of the Inco family of companies.
[h]Watlow G8A53-NT96.
[i]Invar, model #TP 36-18.
[j]Fluke 8600A.

where P_{in} is the input power; P_{xs} is the excess power generated (the source of this power is described later in this paper); and P_{loss} is the thermal power loss from the cell. In these experiments, the applied voltage V_{appl} was an intermittent square wave with current I only during the high-voltage interval of the cycle. Thus, the input power is given by

$$P_{in} = (V_{appl} I) Dc \ , \tag{4}$$

where Dc is the duty cycle—the pulse length divided by the period.

When an aqueous solution is electrolyzed to liberate hydrogen and oxygen gases, the input power can be partitioned into two terms:

$$P_{in} = P_{ohm} + P_{gas} \ , \tag{5}$$

where P_{ohm} is the ohmic power that heats the cell and P_{gas} is the power needed to produce the H_2 and O_2 gases.

$$H_2O(l) \rightarrow H_2(g) + \tfrac{1}{2}O_2(g) \ . \tag{6}$$

An expression for P_{gas} ($= V_{gas} I$) is readily obtained from the known enthalpy of formation of water ($\Delta H_f = -286$ kJ/mol):

$$V_{gas} = -\frac{\Delta H_f}{\alpha F} = -\frac{-286 \times 10^3 \text{ J/mol}}{2 \times 96\,484 \text{ C/mol}} = 1.48 \text{ V} \ , \tag{7}$$

where α is the number of moles of electrons involved in the reaction and F is the faraday constant. The net faraday efficiency of gas evolution is assumed to be unity. Thus, the ohmic power is given by

$$P_{ohm} = (V_{appl} - 1.48) IDc \ . \tag{8}$$

The thermal power loss from the cell can be partitioned into two terms:

$$P_{loss} = P_{cdr} + P_{other} \ , \tag{9}$$

where P_{cdr} is the power lost to the condenser and P_{other} is other power losses (e.g., hot gases that escape through the condenser before reaching thermal equilibrium; conductive heat losses from the cell to the room). Power losses to the condenser, P_{cdr}, are given by

$$P_{cdr} = vC_p(T_O - T_I) \ , \tag{10}$$

where v is the flow rate of the water through the condenser; C_p is the specific heat of water at constant pressure (4.184 J/g·K); T_I is the temperature of the condenser-water at the inlet; T_O is the temperature of the condenser-water at the outlet.

Power losses other than to the condenser were determined with no electrolysis processes occurring by turning on an internal resistance heater to give a cell temperature of 50°C and inferring the efficiency eff from the ratio of the measured condenser losses to the power dissipated in the heater P_{htr}.

$$P_{htr} = V_{htr} I_{htr} \tag{11}$$

$$eff = \frac{P_{cdr}}{P_{htr}} = \frac{vC_p(T_O - T_I)}{P_{htr}} \ . \tag{12}$$

This method overestimates the efficiency because there is no electrolysis gas flow (which adds to the heat losses other than to the condenser).

During electrolysis, then, the output power P_{out} is given by

$$P_{out} = \frac{P_{cdr}}{eff} \ . \tag{13}$$

Data points (V_{appl}, I, Dc, v, T_O, T_I, V_{htr}) were taken every two min. The total energy input E_{in} is the summation over n data points of input power × time intervals Δt_i. The value P_{in} for each data point is given by Eq. (4) for the electrolysis experiments and by Eq. (11) for the resistance heater experiments:

$$E_{in} = \sum_1^n (P_{in})_i \Delta t_i \ . \tag{14}$$

Similarly, the total energy output E_{out} is the summation over n data points of output power × time intervals Δt_i, where P_{cdr} for each data point is given by Eq. (10):

$$E_{out} = \frac{1}{eff} \sum_1^n (P_{cdr})_i \Delta t_i \ . \tag{15}$$

II.B. Electrolysis Methods

Each cathode was a 30.5-cm-wide × 122-cm-long 100 × 100 mesh, 0.0051-cm-diam nickel 200 wire cloth[k] that was sewed on one long edge with 0.38-mm-diam nickel wire to a 244-cm-long, 6.35-mm-diam nickel 200 rod[l] that also served as the lead. Each cathode was cleaned by placing it in the glass test tube liner containing 0.57 M X_2CO_3/3% H_2O_2, X = K for the K_2CO_3 experiments and X = Na for the Na_2CO_3 experiments, for 30 min and then rinsed with distilled water.

Each anode was a 20-cm-wide × 100-cm-long × 0.080-in.-thick nickel fiber mat with 0.80 g of NiO per square inch[m] that was sewed on one long edge with 0.38-mm-diam nickel wire to a 244-cm-long, 6.35-mm-diam nickel 200 rod[l] that also served as the lead. The anodes were cleaned as mentioned earlier for the cathodes. The anode sheet was wrapped around the cathode and a 1-mm-thick Teflon mesh sheet was inserted to prevent contact between the cathode and the anode.

As usual in electrochemistry, measures were taken to avoid impurities in the system, especially organic substances. We note here the known problems with the

[k] Belleville Wire Cloth Co., Inc.
[l] Williams.
[m] National Standard 80/20 Fibrex.

reproducibility of the hydrogen overpotential, which can be overcome only by ensuring the lowest possible level of impurities. The following procedures were used in order to reproduce the excess heat effect. Before starting the experiment, the electrolysis dewar liner was cleaned with Alconox and 0.1 *M* nitric acid and rinsed thoroughly with distilled water to remove all organic contaminants. The nickel cathode and anode were handled with rubber gloves. The electrodes were cut and folded in such a way that no organic substances were transferred to the nickel surfaces. The electrodes were assembled in the glass test tube, which was sealed with the Teflon cap; the leads penetrated the cap. The glass liner containing the electrode assembly was inserted into the dewar, and the condenser was inserted through a perforation in the Teflon cap. The electrode leads were then connected to the power supply, and electrolyte was added under electrolysis voltage. The electrodes were never left in the electrolyte without electrolysis current.

The electrolyte level was maintained to full by additions of distilled water through the condenser (to replace water lost through electrolysis). A drop in the electrolyte level of 50 ml below full was indicated by an open circuit resistance reading of two nickel leads that penetrated the Teflon cap.

A Kepco ATE-100M constant current supply was programmed at 15.0-A peak current (±0.05%) and driven by a function generator[n] to produce a square wave. The time average voltage, current, and power were measured with a digital V-A-W meter.[o] The voltage, current, and power readings of the power meter, as well as the temperature data of the microprocessor thermometers were acquired every 2 min over the duration of the experiment by the data acquisition system—an Apple Mac II SI 5/80 with a NU bus adapter and the following G W Instruments, Inc. hardware: GWI-625 Data Acquisition Board; GWI-J2E Multiplexer; GWI-ABO Analog Breakout System; GWI-34W Ribbon cable. The peak current was determined from the voltage measurement (±0.1%) across an Ohio Semitronics CTA 101 current transducer. The peak voltage, offset voltage, duty cycle, and frequency measurements were made with an oscilloscope.[p]

For experiment 1, the electrolyte solution was 11 ℓ of 0.57 *M* aqueous K_2CO_3 (Aldrich $K_2CO_3 * \frac{3}{2}H_2O$ 99+%). The current-voltage parameters were as follows: a periodic square-wave having an offset voltage of 1.51 V (1.51 V was applied at zero current); a peak voltage of 2.10 V; a peak constant current of 15.0 A; a 15.0% duty cycle; a frequency of 1 Hz. Experiment 1 was run for 14 days. Experiment 1A was the calibration of the efficiency of heat transfer to the condenser for Experiment 1 without electrolysis. Experiment 1A was run for 7 days.

For Experiment 2, the electrolyte solution was 11 ℓ of 0.57 *M* aqueous Na_2CO_3 (Aldrich Na_2CO_3 A.C.S. primary standard 99.95+%). The current-voltage parameters were as follows: a periodic square-wave having an offset voltage of 1.49 V(1.49 V was applied at zero current); a peak voltage of 2.01 V; a peak constant current of 15.0 A; a 15.0% duty cycle; a frequency of 1 Hz. Experiment 2 was run for 7 days. Experiment 2A was the calibration of the efficiency of heat transfer to the condenser for Experiment 2 without electrolysis. Experiment 2A was run for 7 days.

II.C. Calorimetry and Electrolysis Results

The calorimetry parameters, the electrolysis parameters, and the results of Experiments 1 and 2 are given in Table I. The calorimetry parameters and the results of the efficiency determinations, Experiments 1A and 2A, are given in Table II.

For Experiment 1, the cell was disassembled and inspected after 14 days of continuous operation. This inspection showed no visible signs of a reaction between the electrodes and the electrolyte. The pH, specific gravity, concentration of K_2CO_3, and the elemental analysis of the electrolyte sample taken after 14 days of continuous operation were unchanged from that of the values obtained for the electrolyte sample taken before operation, see Table III. Results of elemental analysis of a sample of the nickel cathode taken before operation of the cell and a sample taken immediately after day 14, Table IV, showed that the nickel cathode had not changed chemically. Photomicrographs of a sample of the nickel cathode taken before operation and a sample taken immediately after day 14, Fig. 2, were identical, indicating that the nickel cathode had not changed physically. The water volume added to the cell per 24 h to maintain a constant fill level was 19.1 ml. The volume consumed by faraday losses (conversion to H_2 and O_2) is calculated to be 18.3 ml. Thus, the maintenance water volume exceeded the faraday losses by 4.4% due to loss by atomization (small water droplets swept out of the system) during electrolysis.

II.D. Discussion

The following can be seen from Tables I and II:

1. Substantial excess power was produced during the electrolysis of the aqueous potassium carbonate. The average output power of 24.6 W exceeded the average ohmic power of 1.40 W by a factor >17. During the electrolysis of the aqueous sodium carbonate, however, the output power and the ohmic power were comparable, 1.08 and 1.19 W, respectively. The excess power in the case of aqueous potassium carbonate cannot be attributed to recombination of the evolved hydrogen and

[n]BK Precision Dynascan Corporation, model 3011.
[o]Clarke-Hess Communications Research Corp., model 259 power meter Dc to 30 kHz with an IEEE-488 bus option and a 50-A shunt for Dc to 1 kHz.
[p]Tektronix 10-MHz storage oscilloscope T912.

TABLE I

Input and Output Parameters for the Electrolysis of 0.57 M K_2CO_3 and 0.57 M Na_2CO_3*

Experiment	Solution	V_{appl} ±0.01 V	P_{in} ±0.10 W	P_{ohm} ±0.04 W	Duration (days)	E_{in} ±0.12 MJ	Average P_{cdr} (W)	Average P_{out} (W)	$\frac{P_{out}}{P_{ohm}}$	E_{out} (MJ)
1	K_2CO_3	2.10	4.73	1.40	14	5.72	24.5 ± 0.4	24.6 ± 0.5	17.6	29.8 ± 0.4
2	Na_2CO_3	2.01	4.52	1.19	7	2.73	1.08 ± 0.02	1.08 ± 0.02	0.91	1.31 ± 0.02

*Here, $I = 15.0 \pm 0.1$ A, $Dc = 0.150 \pm 0.003$, and $eff = 0.996 \pm 0.012$.

TABLE II

The Power Input and Output Parameters for the Determination of the Efficiency of Heat Transfer from the Electrolyte to the Condenser

Experiment	Solution	V_{htr} ±0.01 V	I_{htr} ±0.001 A	P_{htr} ±0.01 W	Duration (days)	E_{in} ±0.01 MJ	P_{cdr} ±0.10 W	Efficiency ±0.012
1A	K_2CO_3	12.34	0.532	6.56	7	3.97	6.54	0.996
2A	Na_2CO_3	12.34	0.531	6.55	7	3.96	6.53	0.997

TABLE III

Chemical Analysis of the K_2CO_3 Electrolyte of Experiment 1 Before and After 14 Days of Operation

Flame emission spectrographic analysis	
Mainly	Potassium
Slight trace (100 to 1000 ppm)	Sodium
Very slight trace (<10 ppm)	Magnesium
Specific gravity = 1.062	
Concentration = 0.63 M K_2CO_3	
Solution pH = 11.1	

TABLE IV

Flame Emission Spectrographic Analysis of the Nickel Cloth Cathode of Experiment 1 Before and After 14 Days of Operation

Mainly	Nickel
Trace (0.1 to 0.5%)	Magnesium
Slight trace (100 to 1000 ppm)	Copper
Very slight trace (10 to 100 ppm)	Manganese
Very, very, slight trace (<10 ppm)	Titanium, sodium, silver, aluminum, iron, chromium, silicon

oxygen gases because the average output power greatly exceeded the average input power (by a factor >5).

2. Substantial excess energy was produced during the electrolysis of the aqueous potassium carbonate. The energy output of 29.8 MJ exceeded the energy input of 5.72 MJ by 24 MJ. For the electrolysis of the aqueous sodium carbonate, however, the energy output was considerably less than the energy input. This is the expected result because most of the input energy is consumed in the conversion of water to H_2 and O_2.

3. The excess power and energy that is produced during the electrolysis of aqueous potassium carbonate cannot be attributed to an error in the measurement of the efficiency, 0.996 (Table II). If anything, this value is too high. During electrolysis the evolving hydrogen and oxygen gases must contribute to heat losses other than to the condenser and the efficiency is, undoubtedly, closer to the ratio P_{cdr}/P_{ohm} in experiment 2; 1.08 W/1.19 W or 0.91.

Given these observations and (a) that the potassium ion and the sodium ion are chemically similar, (b) that the anion in the electrolyte was always constant (always carbonate), (c) that the composition of the nickel cathode used in the aqueous potassium carbonate electrolyte was the same before and after the electrolysis (as determined by elemental analysis), and (d) that chemical analysis for potassium ion, carbonate ion, pH, and specific gravity indicated no change in the electrolyte as a result of the electrolysis—we conclude that excess heat and energy were produced in the electrolysis of aqueous potassium carbonate and that no chemical reaction involving the electrodes or the electrolyte is the source of that excess heat.

Similar excess heat results have been reported by Mills[4,5] and others.[6,7]

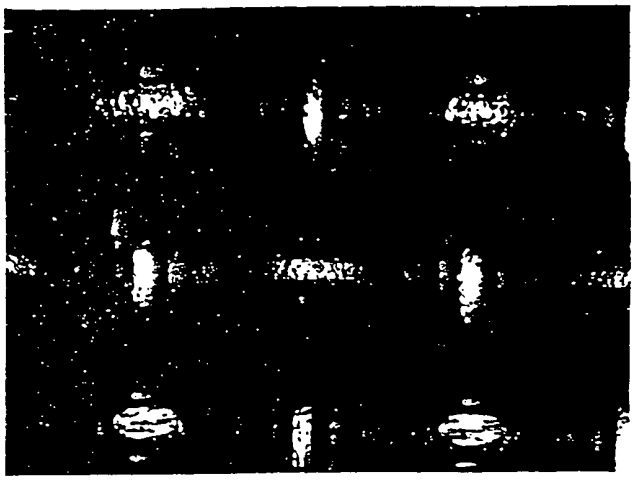

88×

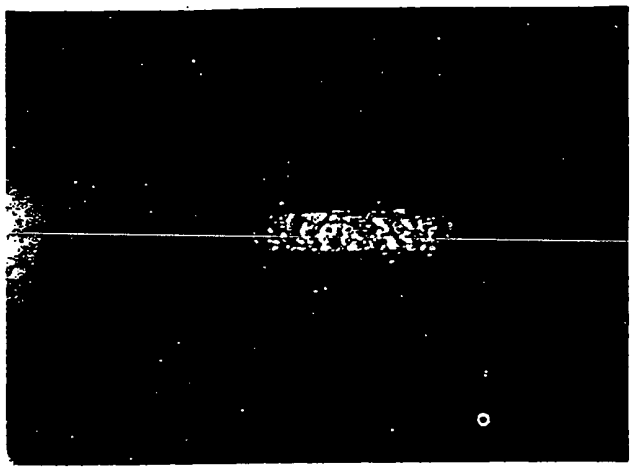

176×

Fig. 2. Photomicrographs of metallurgical samples of the nickel 200 wire cloth (cathode) taken at day 14 of continuous operation.

II.E. Relationship to Fractional Quantum Energy Levels of Atomic Hydrogen

Excess energy during the electrolysis of water in the presence of potassium ions but not in the presence of sodium ions is consistent with an electrocatalytic, exothermic reaction whereby the electrons of hydrogen atoms are induced to undergo transitions to quantized energy levels of lower energy than the conventional "ground state." These lower energy states correspond to fractional quantum numbers as given in Eqs. (2a) and (2c). According to the novel atomic theory,[1,2] transitions of atomic hydrogen ($n = 1$) to these lower energy states are stimulated by the presence of *resonant energy holes* (energy sinks or means to remove energy) of 27.2 eV (the potential energy of a hydrogen atom in the $n = 1$ state; derivation in Refs. 1 and 2). Transitions to these lower energy states occur with the release of energy and with a commensurate decrease in size of the hydrogen atom,[1,2] $r_n = na_H$. For example: the transition $H(n = 1)$ to $H(n = \frac{1}{2})$ releases 40.8 eV, see Eq. (2a), and the hydrogen radius decreases from a_H to $\frac{1}{2}a_H$. An energy hole that is an efficient catalytic system for these atomic hydrogen transitions involves the potassium ion, K^+. The second ionization energy of potassium is 31.63 eV (vacuum level); this energy hole is too high for resonant absorption of 27.2 eV. However, K^+ releases 4.34 eV (vacuum level) when it is reduced to K. The combination of K^+ to K^{2+} and K^+ to K, then, has a net energy change of 27.28 eV (vacuum level). Thus, the stimulated transition can be written as

$$27.28 \text{ eV} + K^+ + K^+ + H(n = 1, r = a_H) \rightarrow K + K^{2+} + H\left(n = \frac{1}{2}, r = \frac{a_H}{2}\right) + 40.8 \text{ eV} . \quad (16)$$

The K atom and the K^{2+} ion will transfer an electron with the release of energy:

$$K + K^{2+} \rightarrow K^+ + K^+ + 27.28 \text{ eV} . \quad (17)$$

The overall, catalytic reaction is

$$H(n = 1, r = a_H) \rightarrow H\left(n = \frac{1}{2}, r = \frac{a_H}{2}\right) + 40.8 \text{ eV} . \quad (18)$$

Thus, each ($n = 1$) hydrogen atom that undergoes this transition releases a net of 40.8 eV. Additional catalytic transitions are possible: $n = \frac{1}{2} \rightarrow \frac{1}{3}$, $\frac{1}{3} \rightarrow \frac{1}{4}$, $\frac{1}{4} \rightarrow \frac{1}{5}$, and so on.

These transitions are, apparently, taking place on the nickel cathode during the electrolysis of aqueous potassium carbonate. Atomic hydrogen is produced at the cathode surface during the electrolysis (part of the process of reducing H_2O to H_2). The juxtaposition of the hydrogen atoms and potassium ions in the electrolyte is an ideal configuration for the catalytic transition of hydrogen to fractional quantum energy levels. The observed "excess heat" is, we suggest, a consequence of these atomic hydrogen transitions.

Neglect, for the moment that $H(n = \frac{1}{2})$ can form a diatomic molecule (called a dihydrino; Sec. V of this paper). Equation (18) predicts that 40.8 eV is released per H atom transition to the $n = \frac{1}{2}$ quantum state, which corresponds to 8 MJ/mol of H_2. In contrast, only 286 kJ is consumed by electrolyzing 1 mol of H_2O to produce 1 mol of H_2, see Eq. (6). Thus, the excess energy produced in experiment 1 of 24 MJ (which also produces 14.1 mol of H_2) could be accounted for by the conversion of 21% of the hydrogen atoms from the $n = 1$ state to the $n = \frac{1}{2}$ state.

For sodium ions, no electrocatalytic reaction of ~27.2 eV is possible and the analogous reaction for sodium is not an appropriate catalytic reaction to produce

lower energy hydrogen atoms. For example, 42.15 eV of energy is absorbed by the reverse of the reaction given in Eq. (17) where Na^+ replaces K^+:

$$Na^+ + Na^+ + 42.15\ eV \rightarrow Na + Na^{2+} \quad . \qquad (19)$$

Almost all electrolysis experiments will be similar to the case of Na_2CO_3, which does not provide an energy hole of ~27.2 eV. Only a few combinations of electrolytes/electrodes, such as the K_2CO_3 case mentioned earlier, provide an energy hole of approximately 27.2 eV, Eqs. (16), (17), and (18), and will yield excess heat.

TABLE V

Binding Energies of the Hydrino Atom as a Function of Principal Quantum Number, Eq. (22)

n	E (eV)
1	13.6
$\frac{1}{2}$	54.4
$\frac{1}{3}$	122.4
$\frac{1}{4}$	217.6

III. IDENTIFICATION OF HYDRINOS—HYDROGEN ATOMS IN FRACTIONAL QUANTUM ENERGY LEVELS—BY XPS

The X-ray photoelectron spectroscopy (XPS) is capable of measuring the binding energy, E_b, of each electron of an atom. A photon source with energy $E_{h\nu}$ is used to ionize electrons from the sample. The ionized electrons are emitted with energy $E_{kinetic}$:

$$E_{kinetic} = E_{h\nu} - E_b - E_r \ , \qquad (20)$$

where E_r is a negligible recoil energy. The kinetic energies of the emitted electrons are measured by measuring the magnetic field strengths necessary to have them hit a detector. The values $E_{kinetic}$ and $E_{h\nu}$ are experimentally known and are used to calculate E_b, the binding energy of each atom. Thus, XPS can provide an incontrovertible identification of an atom.

The binding energy of various hydrino states is easily calculated, Eq. (21) and Table V. The technique of XPS was used to search for the $n = \frac{1}{2}$ hydrino, $E_b = 54.4$ eV, because it is closest in energy to the $n = 1$ state of hydrogen and, therefore, predicted to be the most abundant:

$$E_b = \frac{1}{n^2} 13.6\ eV \qquad n = \frac{1}{2}, \frac{1}{3}, \frac{1}{4}, \cdots \ . \qquad (21)$$

III.A. Experimental Method

A series of XPS analyses have been made on (a) nickel cathodes used in electrolysis of aqueous potassium carbonate and aqueous sodium carbonate, (b) precursor (nickel) electrode material, and (c) various standards. The XPS was performed by the Zettlemoyer Center for Surface Studies, Lehigh University.

The instrument conditions were similar for all of the analyses. In all cases a high quality spectrum was obtained over a minimum binding energy range of 80 to 0 eV. This energy region completely covers the Ni 3p region and the region around 55 eV, which is the approximate location of the $H(n = \frac{1}{2})$ binding energy, 54.4 eV.

Each electrode was removed from the cell while maintaining the electrode overvoltage, rinsed immediately with distilled water, and dried with a N_2 stream. A piece of suitable size was cut from the electrode, mounted on a sample stub, and placed in the vacuum system. Fourteen nickel cathode samples were analyzed by XPS. Each had a slightly different history: two different laboratories ran the electrolyses; nickel foil and nickel wire were used; 99+% and 99.999% K_2CO_3 were used in the electrolyte; 99.95% Na_2CO_3 was used in the electrolyte; some were electrolyzed with simultaneous calorimetric measurements and others were not; some were analyzed immediately after electrolysis and some were stored in liquid N_2 before analysis. A brief description of the preparation conditions for each of the samples discussed in this manuscript is given as follows:

Sample 1: Nickel foil. K_2CO_3 (Alpha 99+%) electrolyte. Platinum anode. No calorimetry performed during electrolysis.

Sample 9: Nickel wire. K_2CO_3 (Puratronic 99.999%) electrolyte. Nickel anode. The K_2CO_3 electrolyte was further purified by preelectrolyzing: the electrolyte was prepared and electrolyzed with a "dummy" nickel cathode for 1 month; the "dummy" nickel electrode was then replaced with the nickel wire (sample 9). Calorimetry was performed during electrolysis. Cell was producing "excess" heat.

Sample 14: Nickel wire. Na_2CO_3 (99.95%) electrolyte. Nickel anode. The Na_2CO_3 electrolyte was further purified by preelectrolyzing as described for sample 9. Calorimetry was performed during electrolysis. Cell was not producing "excess" heat.

Specimens of pure elements and the passivation oxides of these elements that were analyzed to provide standards were not given sample numbers. The preparation conditions for these specimens are listed on the figures or given in the figure captions.

III.B. Results and Discussion

A survey spectrum of sample 1 is shown in Fig. 3. The primary elements are identified on the figure. Most of the unidentified peaks are secondary peaks or loss features associated with the primary elements. Tin is clearly a major contaminant of the surface composition.

Figure 4 shows the low binding energy range for sample 1. Again, tin is seen to be a major surface contaminant. Magnesium and chromium are also present. The broad peak labeled X is the one of most interest because it falls near the predicted binding energy for the hydrino ($n = \frac{1}{2}$), 54.4 eV. It has a full-width at half-maximum (FWHM) of about 5.1 eV, and it is centered at a binding energy of 54.6 eV. It is important to note that binding energies in XPS are measured relative to the fermi level, not to the vacuum level. Although the agreement is remarkable, it was necessary to eliminate all other possible explanations before assigning the X feature to the hydrino. Elements that potentially could give rise to a peak near 55 eV can be divided into three categories: fine structure or loss features associated with one of the four major surface components—nickel, platinum, tin, zinc; elements that have their primary peaks in the vicinity of 55 eV—lithium; elements that have their secondary peaks in the vicinity of 55 eV—iron. To examine these possibilities, several experiments were performed.

Nickel. Nickel was the cathode material. Figure 5 shows an expanded scale spectrum of (unused) nickel foil material that has undergone a variety of treatments ranging from clean metal (scraped in vacuum) to room temperature oxidation in pure O_2 (30 kPa for 15 min at room temperature) to air passivation at room temperature. Examination of this figure shows no evidence for any spectral features in the range of interest. The X feature is not from nickel or nickel oxide.

Platinum. Platinum was the anode material in the electrolysis and was found in the survey spectrum of sample 1. The Pt $5p_{3/2}$ falls at 51.4 eV—close to the 54.6 eV feature and close to the predicted binding energy of the hydrino, 54.4 eV. From a spectrum of pure platinum, it was determined that the area ratio of the Pt $5p_{3/2}$ peak to the total Pt 4f peak is 0.043. In the spectrum of sample 1, the area ratio of the X feature to the Pt 4f peaks is 0.75. The area of X is about 17 times too large to attribute the peak to platinum. Furthermore, Fig. 6 shows that the platinum peak position does not match that of feature X; platinum is eliminated.

Tin. Tin was found in the survey spectrum of sample 1. Figure 6 superimposes four spectra: sample 1, clean tin metal, thick tin oxide, and platinum metal. Clean tin metal has a bulk plasmon peak at −53 eV. However, this plasmon peak is several times weaker than the plasmon at 38.7 eV. The 38.7-eV peak does not appear in the spectrum of sample 1. Thus, the X feature cannot be assigned to tin metal. The thick tin oxide spectrum shows no structure in this energy range. Comparison of the tin peaks in sample 1 and the tin oxide peaks indicate that most of the tin signal is from oxidized tin. Feature X is not from tin or tin oxide.

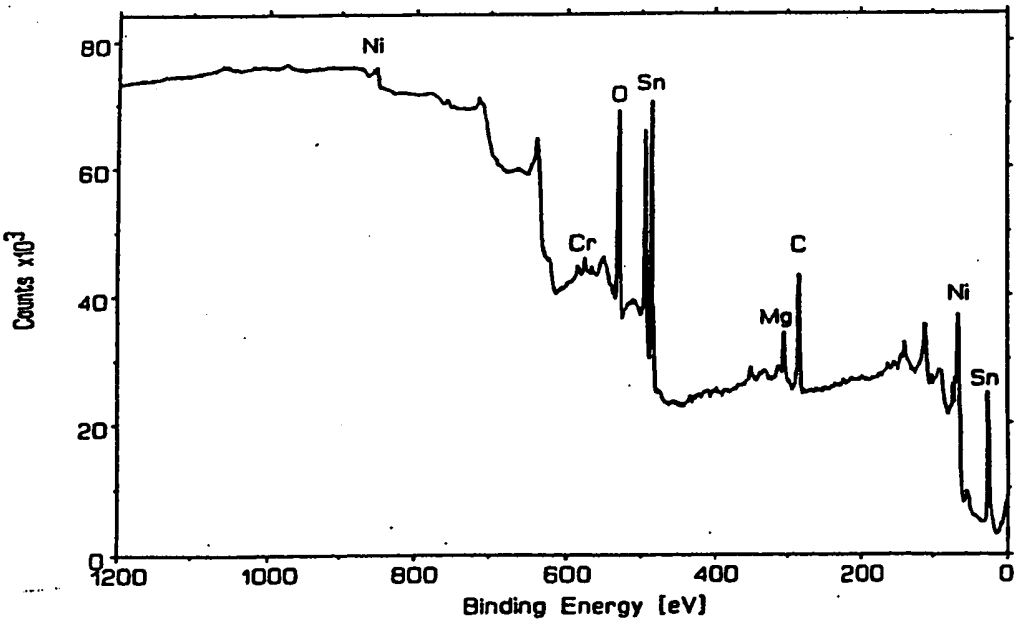

Fig. 3. The XPS survey spectrum of nickel (foil) sample 1. Primary impurity elements are identified.

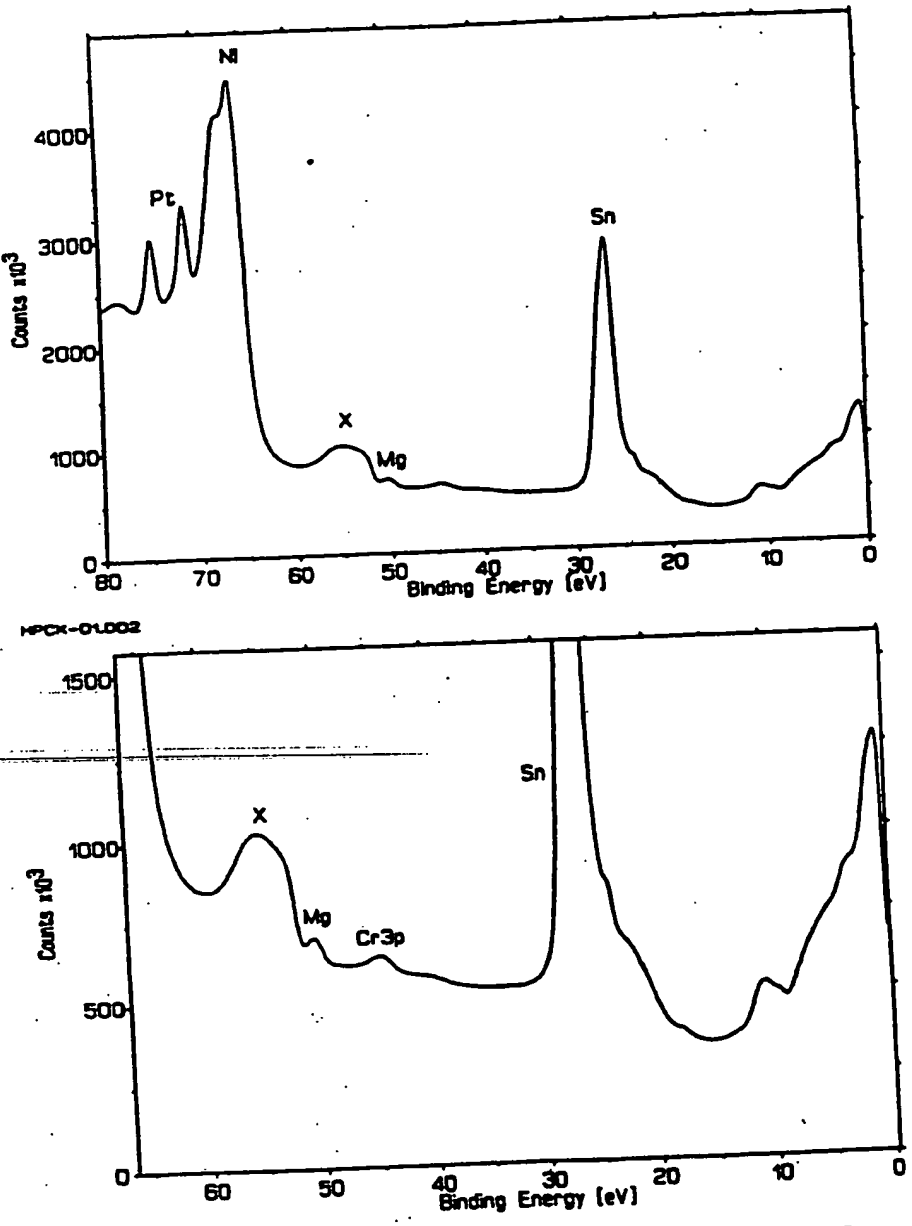

Fig. 4. The XPS spectrum of nickel sample 1 in the low-energy region. It shows feature *X* centered at 54.6 eV.

Zinc. Zinc was found in the survey spectrum of sample 1. Zinc was eliminated using similar arguments as those used to eliminate tin, see Fig. 7.

Lithium. First, the lithium 1s peak is several eV below that of feature *X*. Second, if feature *X* was due to lithium, the lithium would be in the form of lithium oxide and the oxide peak would be off scale. Third, the Li 1s peak is quite narrow whereas feature *X* is broad. Fourth, a sample of the nickel was analyzed by time-of-flight secondary ion mass spectroscopy (TOF-SIMS), and no lithium was found. Feature *X* is not from lithium.

Iron. Iron has a 3p peak in this region. The primary iron peak, the 2p levels, are obscured by the very strong nickel Auger lines. Spectra of clean nickel and clean iron suggest that iron concentrations of <5% (relative to nickel) should be discernible in the Fe 2p energy region. The intensity of the *X* feature is such that if the *X* feature was assigned as Fe 3p, the iron concentration would be ~10% and the Fe 2p would be discernible from the nickel Auger lines—but it is not. Iron can also be eliminated by noting the shift in binding energy of feature *X* upon heating. Figure 8 overlays three spectra: sample 1, sample 1 heated to ~700°C, and sample 1 stored in air for 26 days. Note that heating

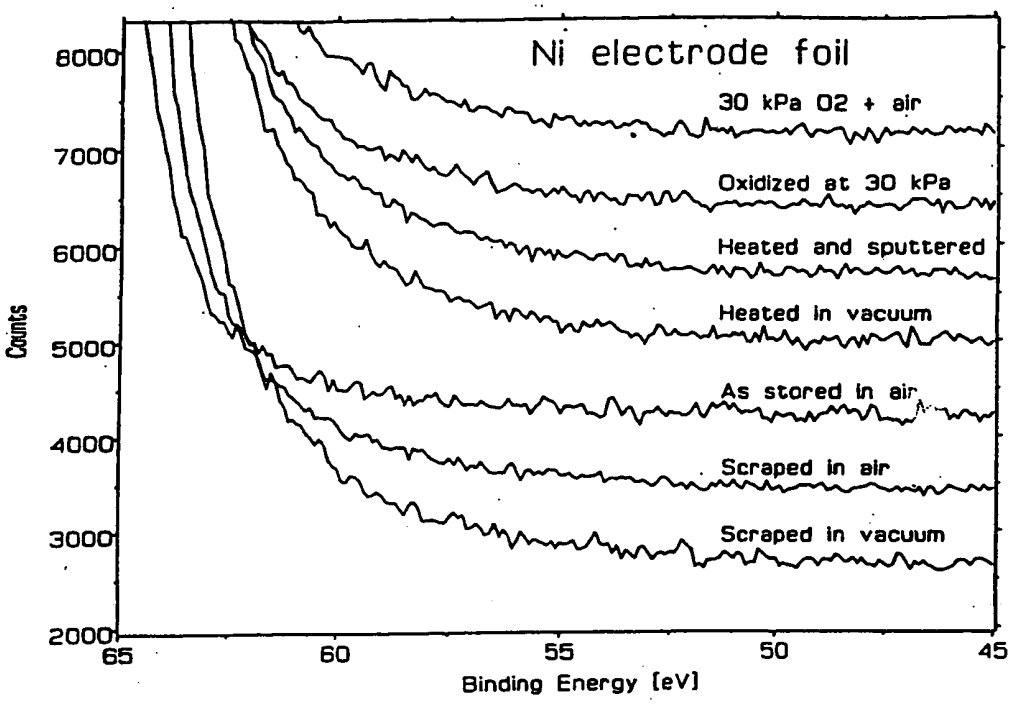

Fig. 5. The XPS spectra of unused nickel foil subjected to various conditioning treatments.

shifts the centroid to a *higher binding energy*. Heating under ultrahigh vacuum (UHV) conditions tends to reduce oxides and shifts peaks to *lower binding energies*. This is clearly evident in Fig. 9 which shows the Sn 4d spectrum of sample 1 before and after heating. If feature X is an Fe 3p peak, the expected result would have been a decrease in the binding energy upon heating. Feature X is not from iron.

To further eliminate the possibility that feature X was due to the impurities mentioned, four additional measures were taken for the conditioning of sample 9:

1. use of a higher purity nickel wire
2. using nickel as the anode (rather than platinum, which was an impurity source in sample 1)
3. use of 99.999% K_2CO_3
4. the potassium was preelectrolyzed (see sample 9 description earlier).

In addition, sample 9 was taken from a calorimeter/electrolysis cell known to be producing more power than the total input power. Only two impurities were found in the survey spectrum of sample 9: potassium, suggesting that the rinsing may not have been complete, and indium at a very low level (undoubtedly from the nickel wire). This sample was also analyzed for iron by electron-dispersive spectroscopy (EDS), Auger, and TOF-SIMS at the Idaho National Engineering Laboratory (INEL)—no iron was found above the detection limit, ~0.1%. The XPS results were confirmed at INEL and Charles Evans & Associates followed by time of flight-secondary ion mass spectroscopy (TOF-SIMS) analysis of the nickel surface at Charles Evans & Associates. The Charles Evans & Associates TOF-SIMS results were negative for iron and negative for lithium. Figure 10 shows the lower binding energy portion of the spectrum for sample 9 (99.999% K_2CO_3). Feature X is closer to 57 eV, but it is very similar in shape to the feature of other nickel samples using aqueous K_2CO_3 as the electrolyte. The spectrum of sample 1 is overlaid for comparison.

As an additional control experiment, nickel from a sodium carbonate cell that was not producing excess heat was examined. Sample 14 is the exact analog of sample 9—except for the difference in electrolyte. The low energy portion of the spectrum of sample 14 (nickel cathode from Na_2CO_3 electrolysis) is shown in Fig. 11. There is only a small trace of magnesium in the region of interest. Feature X is not present and was not found on any spectrum of nickel samples from aqueous Na_2CO_3 electrolysis. Figure 12 is an overlay of the spectra of sample 9 (K_2CO_3) and sample 14 (Na_2CO_3).

In summary:

1. Nickel cathodes used in the electrolysis of aqueous K_2CO_3 (no calorimetry measurements taken) had a broad peak at 54.6 eV—close to the predicted vacuum binding energy of the hydrino ($n = \frac{1}{2}$), 54.4 eV.

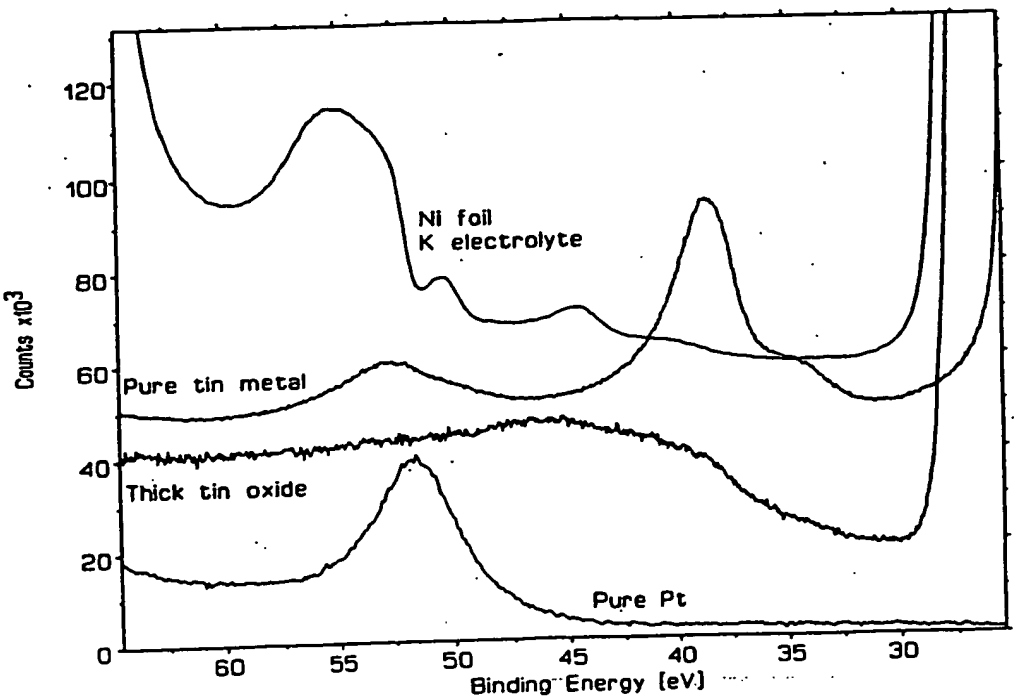

Fig. 6. Overlay of four spectra: sample 1; platinum; tin; tin oxide. These impurities have smaller binding energies than feature *X*.

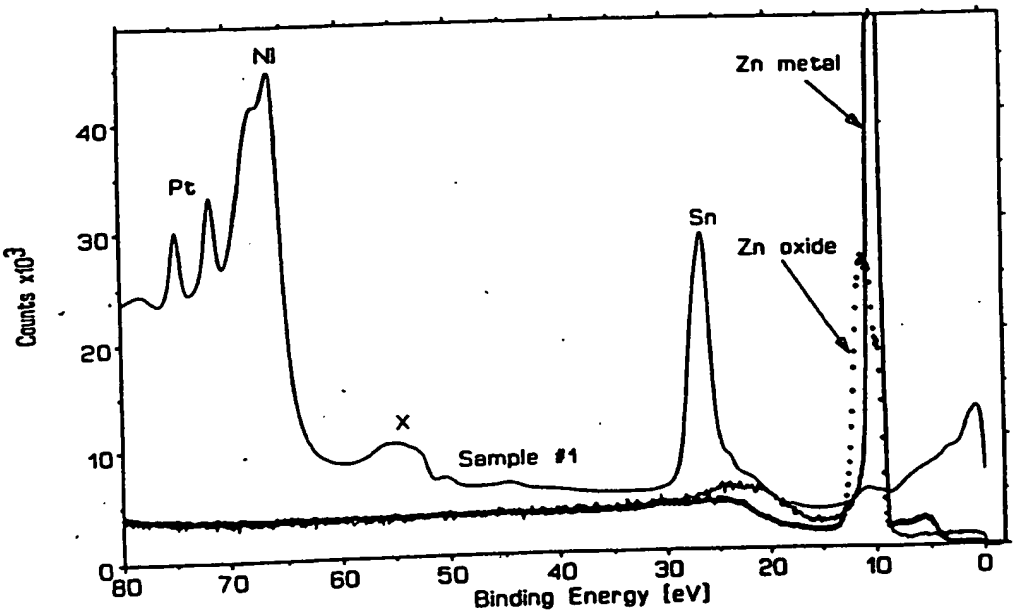

Fig. 7. Overlay of three spectra: sample 1; Zn; ZnO. These binding energies do not match the binding energy of feature *X*.

2. A nickel cathode used in the electrolysis of aqueous K_2CO_3 (99.999%) where calorimetry measurements had shown that the cell was producing more power than the total input power, also had a broad peak close to the predicted binding energy of the hydrino ($n = \frac{1}{2}$), 54.4 eV.

3. Clean nickel, heated nickel, and nickel under various oxidizing conditions did not have a peak in this range.

4. Nickel cathodes used in the electrolysis of aqueous Na_2CO_3 did not have a peak in this range.

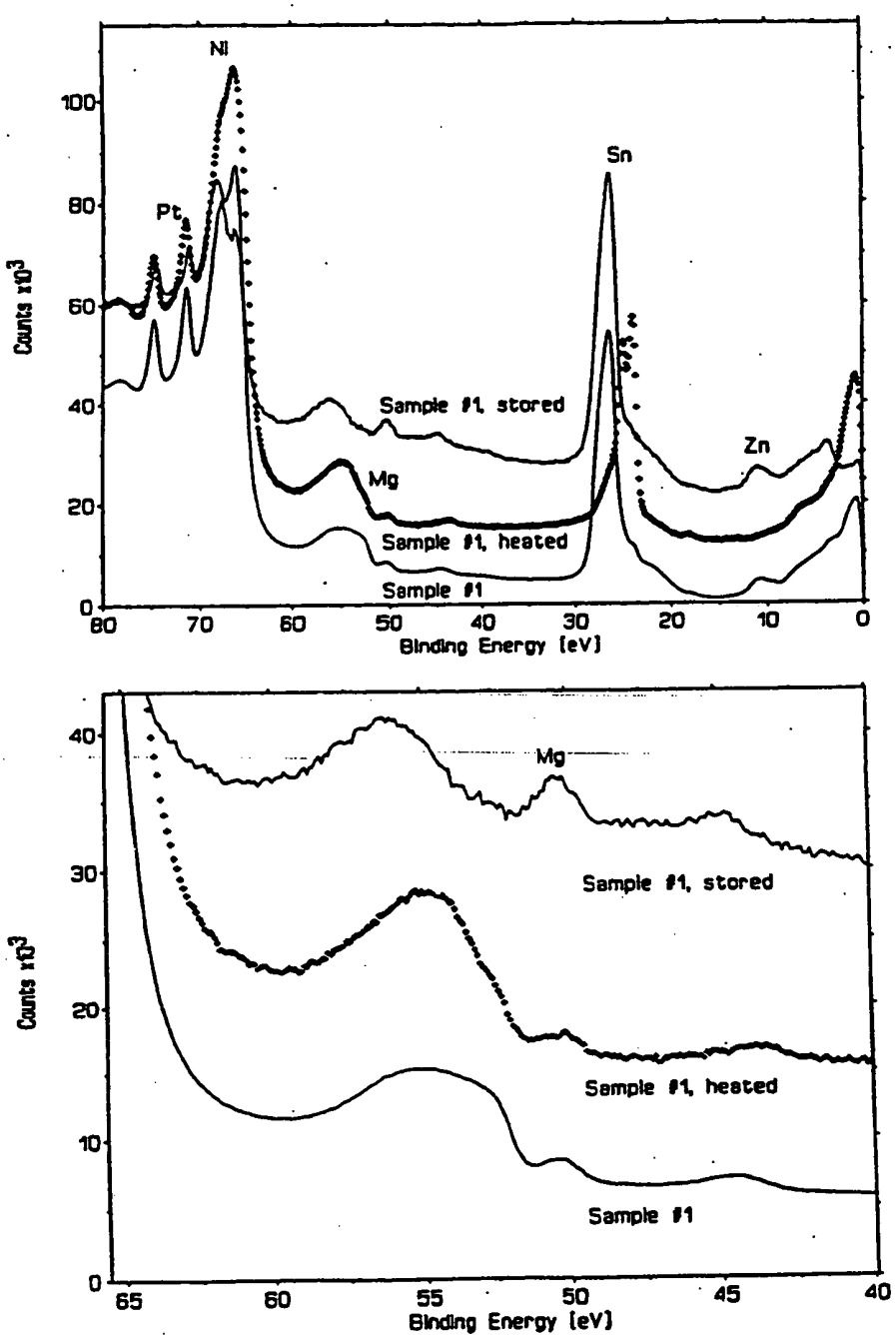

Fig. 8. Overlay spectra: sample 1; sample 1, heated; sample 1, stored. Heating shifts feature X to a higher binding energy.

5. Efforts to identify this peak as one of the surface contaminants or as another element with a primary or secondary peak in this energy range have failed.

The data are consistent with the assignment of the broad 54.6-eV peak to the hydrino, $H(n = \frac{1}{2})$. The abnormal breath of the peak is consistent with the presence of both $H(n = \frac{1}{2})$ and the corresponding molecule described in Sec. V.

IV. IDENTIFICATION OF FRACTIONAL QUANTUM ENERGY LEVELS OF HYDROGEN BY SOFT X RAYS FROM THE DARK INTERSTELLAR MEDIUM

The first soft X-ray background was detected and reported[8] about 25 yr ago. Quite naturally, it was assumed that these soft X-ray emissions were from ionized atoms within hot gases. In a more recent paper, a grazing incidence spectrometer was designed to measure and

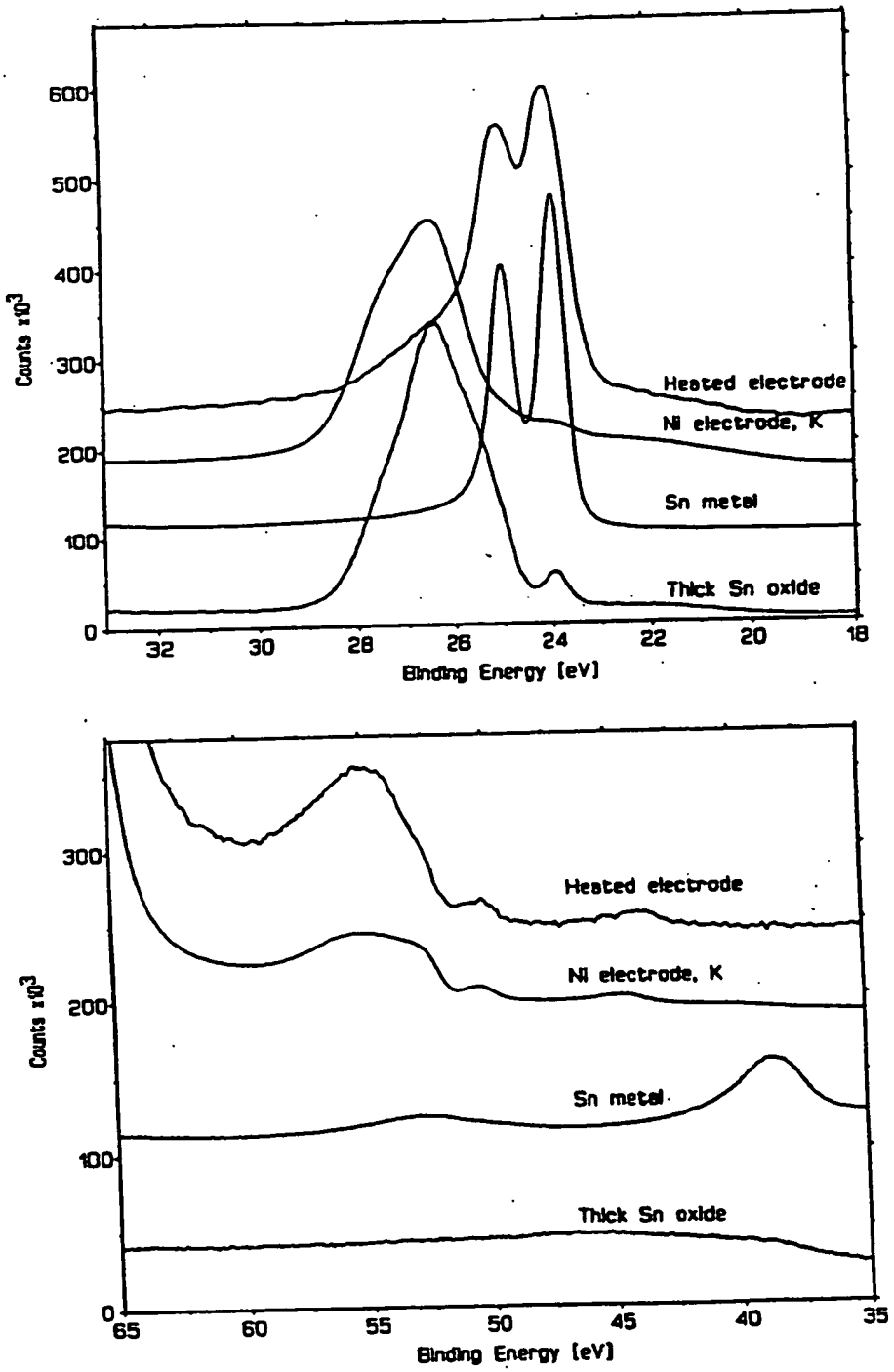

Fig. 9. Overlay spectra showing that heating under UHV tends to reduce metals and shift peaks to lower binding energies.

record the diffuse extreme ultraviolet background.[9] The instrument was carried aboard a sounding rocket, and data were obtained between 80 and 650 Å (data points approximately every 1.5 Å). Here again, the data were interpreted as emissions from hot gases. However, the authors left the door open for some other interpretation with the following statement from their introduction:

> "It is now generally believed that this diffuse soft X-ray background is produced by a high-temperature component of the interstellar medium. However,

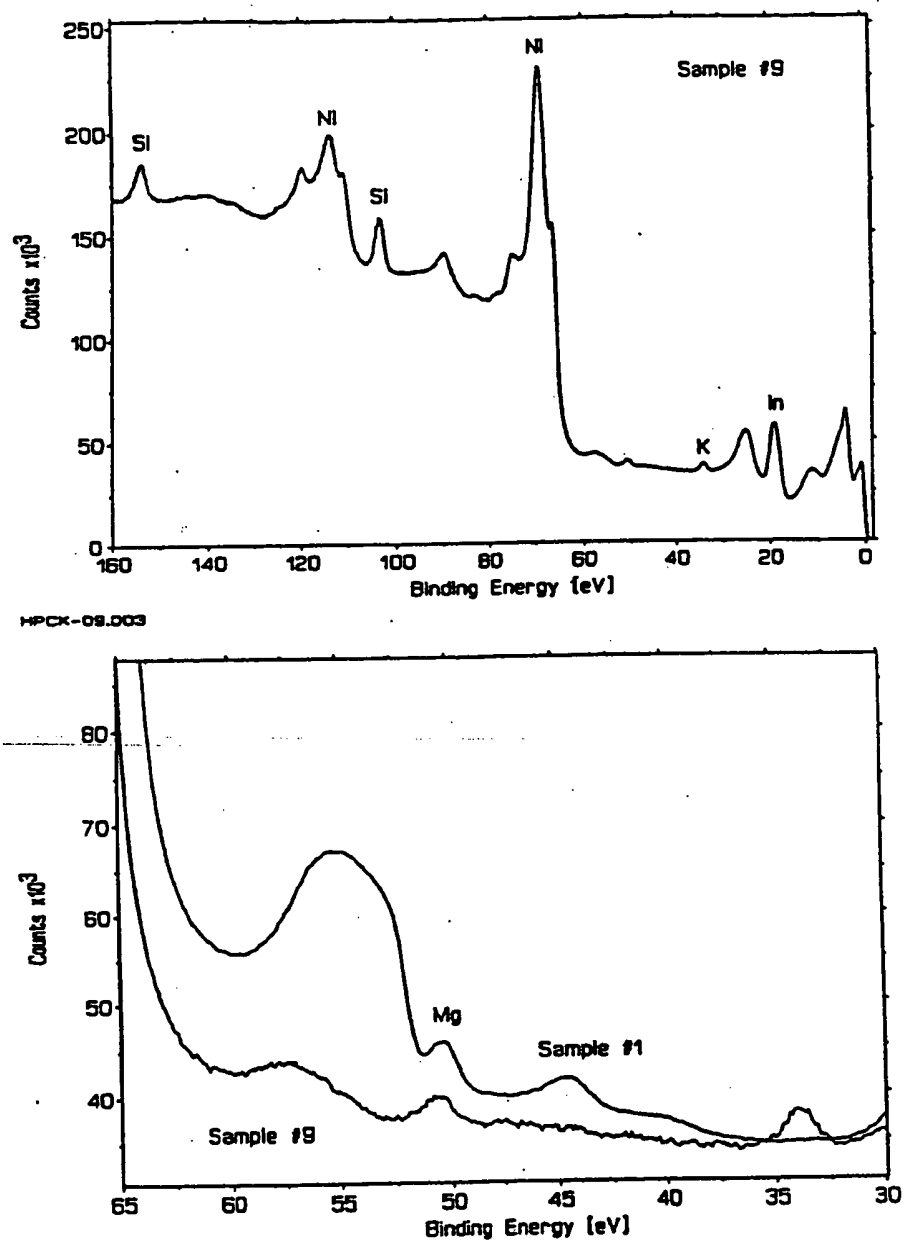

Fig. 10. Survey spectrum of nickel (wire) sample 9 (99.999% K_2CO_3). The sample is much "cleaner" than sample 1.

evidence of the thermal nature of this emission is indirect in that it is based not on observations of line emission, but on indirect evidence that no plausible nonthermal mechanism has been suggested which does not conflict with some component of the observational evidence."

The authors also state that "if this interpretation is correct, gas at several temperatures is present." Specifically, emissions were attributed to gases in three ranges: $5.5 < \log T < 5.7$; $\log T = 6$; $6.6 < \log T < 6.8$.

The explanation proposed herein of the observed dark interstellar medium spectrum hinges on the possibility of energy states below the $n = 1$ state, as given by Eqs. (2a) and (2c). Thus, transitions of the type,

$$\Delta E = 13.60\left(\frac{1}{n_f^2} - \frac{1}{n_i^2}\right)\text{eV} \qquad n = 1, \frac{1}{2}, \frac{1}{3}, \frac{1}{4}, \cdots \qquad n_i > n_f \tag{22}$$

ought to occur. The wavelength is related to ΔE by

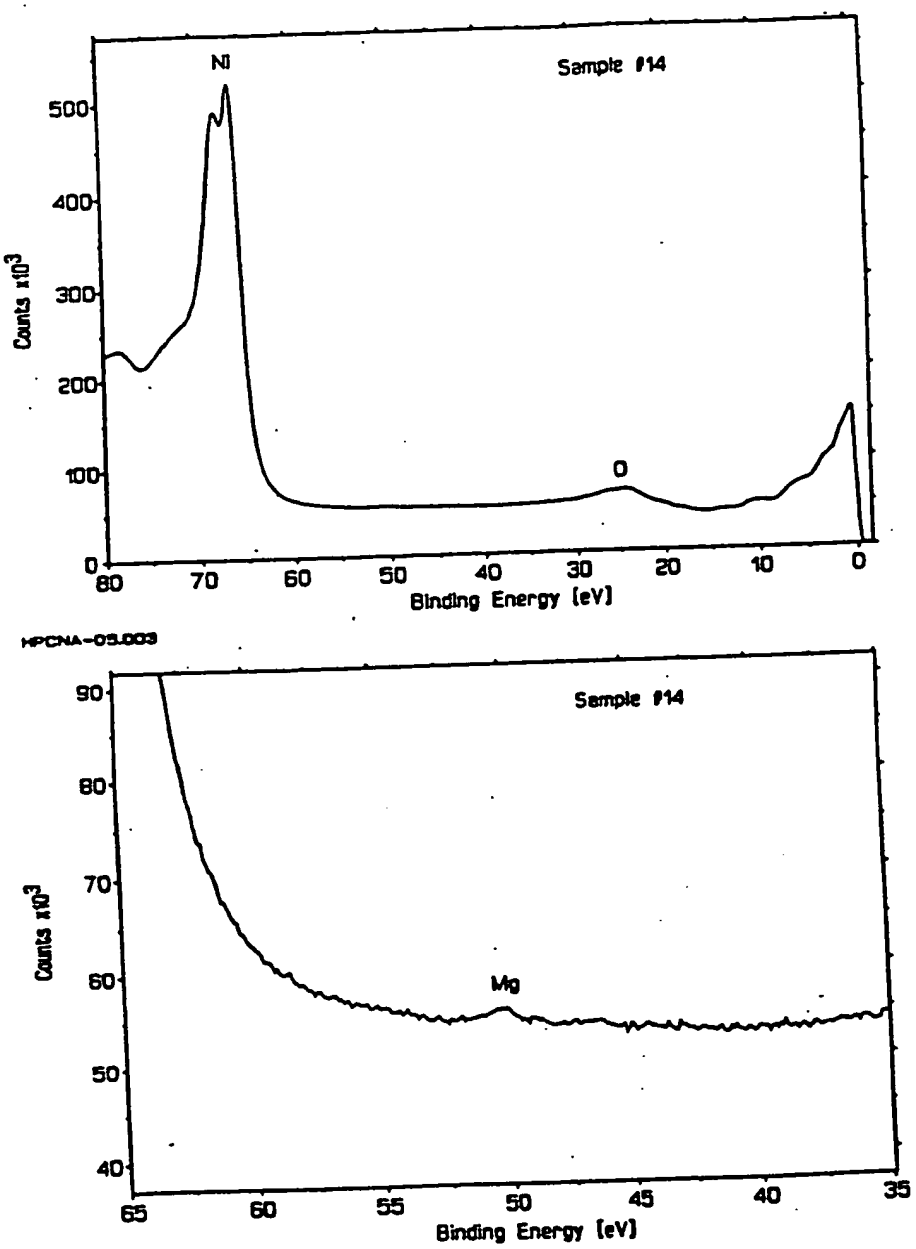

Fig. 11. The XPS spectrum of sample 14 (Na_2CO_3). Feature X is not found.

$$\lambda \text{ (in Å)} = \frac{1.240 \times 10^4}{\Delta E \text{ (in eV)}} \quad . \tag{23}$$

The energies and wavelengths of several of these proposed transitions are shown in Table VI. Note that the lower energy transitions are in the soft X-ray region.

IV.A. The Data and Data Interpretation

In their analysis of the data, Labov and Bowyer[9] established several tests to separate emission features from the background. There were seven features (peaks) that passed their criteria. The wavelengths and other aspects of these peaks are shown in Table VII. Peaks 2 and 5 were interpreted by Labov and Bowyer as instrumental second-order images of peaks 4 and 7, respectively. Peak 3, the strongest feature, is clearly a helium resonance line: $He(1s^1 2p^1 \rightarrow 1s^2)$. At issue here, is the interpretation of peaks 1, 4, 6, and 7. We suggest that peaks 4, 6, and 7 arise from the $1 \rightarrow \frac{1}{2}$, $\frac{1}{2} \rightarrow \frac{1}{3}$, and $\frac{1}{4} \rightarrow \frac{1}{5}$ hydrogen atoms transitions given by Eq. (22). We also suggest that peak 1 arises from helium scattering of peak 4. That is, the $1 \rightarrow \frac{1}{2}$ transition yields a 40.8 eV photon (303.9 Å). When this photon strikes He

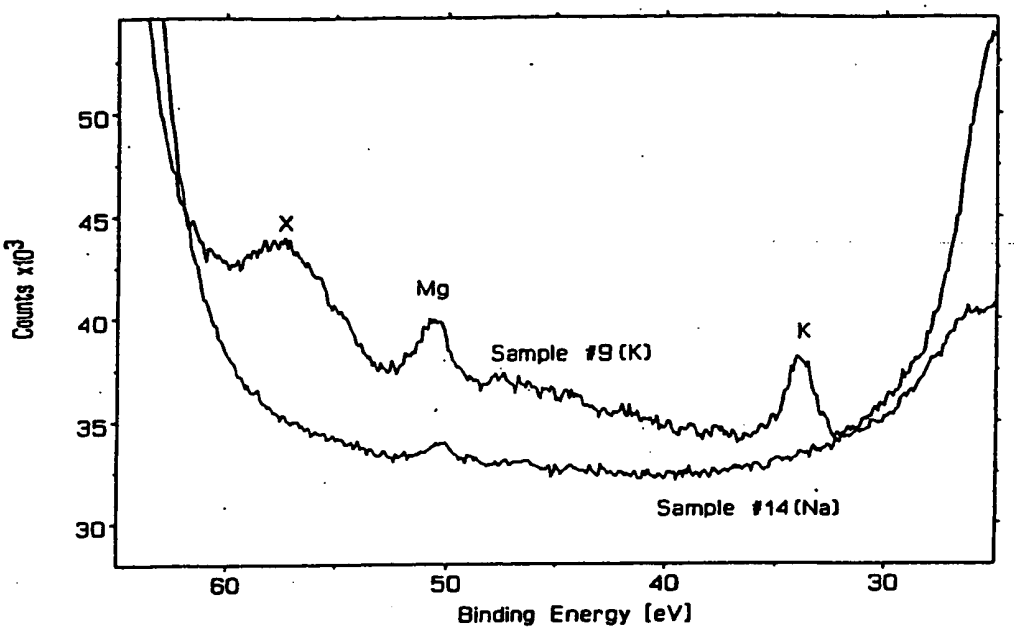

Fig. 12. Overlay of spectra of sample 9 (K_2CO_3) and sample 14 (Na_2CO_3) in the region of interest. Feature *X* is found only in the nickel from the K_2CO_3 electrolysis.

($1s^2$), 21.2 eV is absorbed in the excitation to He ($1s^12p^1$). This leaves a 19.6 eV photon (632.6 Å), peak 1. For these four peaks, the agreement between the predicted values, Table VII, and the experimental values is remarkable.

One argument against this new interpretation of the data is that the transition $\frac{1}{3} \rightarrow \frac{1}{4}$ is missing—predicted at 130.2 Å by Eqs. (22) and (23). This missing peak cannot be explained into existence, but a reasonable rationale can be provided for why it might be missing from these data. The data obtained by Labov and Bowyer are outstanding when the region of the spectrum, the time allotted for data collection, and the logistics are considered. Nonetheless, it is clear that the signal-to-noise ratio is low and that considerable effort had to be expended to differentiate emission features from the background. This particular peak, $\frac{1}{3} \rightarrow \frac{1}{4}$, is likely to be only slightly stronger than the $\frac{1}{4} \rightarrow \frac{1}{5}$ peak (the intensities, Table VII, appear to decrease as *n* decreases), which has low intensity. Labov and Bowyer supplied their data to us (wavelength, count, count error, background, and background error). The counts minus background values for the region of interest, 130.2 ± 5 Å, are shown in Table VIII (the confidence limits for the wavelength of about ±5 Å are the single-side 1 confidence levels and include both the uncertainties in the fitting procedure and uncertainties in the wavelength calibration). Note that the largest peak (count minus background) is at 129.64 Å and has a counts minus background = 8.72. The counts minus background for the strongest signal of the other hydrino transitions are: $n = 1$ to $n = \frac{1}{2}$, 20.05; $n = \frac{1}{2}$ to $n = \frac{1}{3}$, 11.36; $n = \frac{1}{4}$ to $n = \frac{1}{5}$, 10.40. Thus, there is fair agreement with the wavelength and the strength of the signal. This, of course, does not mean that there is a peak at 130.2 Å. However, it is not unreasonable to conclude that a spectrum with a better signal-to-noise ratio might uncover the missing peak.

TABLE VI

Energies of Several Fractional-State Transitions

n_i	n_f	ΔE (eV)	λ (Å)
1	$\frac{1}{2}$	40.80	303.9
$\frac{1}{2}$	$\frac{1}{3}$	68.00	182.4
$\frac{1}{3}$	$\frac{1}{4}$	95.20	130.2
$\frac{1}{4}$	$\frac{1}{5}$	122.4	101.3
$\frac{1}{5}$	$\frac{1}{6}$	149.6	82.9

Another, and more important, argument against this new interpretation is the fact that the proposed fractional-quantum-state hydrogen atoms have not been detected before. There are several explanations. First, the transitions to these fractional states must be forbidden or must have very high activation energies—otherwise all hydrogen atoms would quickly go to these lower energy states (we estimate the transition probability, based on the Labov and Bowyer data, to be between 10^{-15} and 10^{-17} s^{-1}). Second, the number of hydrogen *atoms* ($n = 1$) and the hydrogen-*atom* density

TABLE VII

Emission Features of the LaBov and Bowyer Spectrum and Peak Assignments

Peak	λ (Å)	Confidence Limit (Å)	Intensity (photon/cm²·s·sr)	Assignment[9]	Assignment[5]	Predicted λ (Ref. 5) (Å)
1	634.7	−4.7 to +4.7	19000	O^{4+}; log $T = 5.5$	Helium scattering of 303.9 line (peak 4)	632.6
2	609.1	−4.9 to +4.9	Second order	Second order of 299.7 line	Second order of 303.9 line	607.8
3	582.1	−4.5 to +4.5	70400	Helium resonance ($1s^12p^1 \rightarrow 1s^2$)	Helium resonance ($1s^12p^1 \rightarrow 1s^2$)	584
4	299.7	−6.0 to +5.9	2080	He^+; ($2p^1$ to $1s^1$)	$n = 1$ to $n = \frac{1}{2}$	303.9
5	200.4	−4.4 to +5.3	Second order	Second order of 98.7 line	Second order of 101.3 line	202.6
6	178.1	−4.6 to +5.1	1030	Fe^{9+} and Fe^{10+}; log $T = 6$	$n = \frac{1}{2}$ to $n = \frac{1}{3}$	182.4
7	98.7	−5.3 to +4.2	790	Fe^{17+} and Fe^{18+}; log $T = 6.6$ to 6.8	$n = \frac{1}{4}$ to $n = \frac{1}{5}$	101.3

under any conditions on Earth is exceeding low. The combination of extremely low population and extremely low transition probability makes the detection of these transitions especially difficult. Third—hydrogen atoms in these lower energy states would be very stable, diffuse readily, and have higher (thermal) velocities than helium, which readily escapes from the planet. Fourth, this is a very troublesome region of the electromagnetic spectrum for detection because these wavelengths are significantly attenuated by the atmosphere. Last, no one previously has been actively searching for these transitions.

IV.B. Discussion

We have given an alternative explanation for the soft X-ray emissions of the dark interstellar medium observed by Labov and Bowyer[9] based on the proposed existence of fractional-quantum-energy-level hydrogen atoms, hydrinos. The agreement between the experimental data and the values predicted for the proposed transitions is remarkable. These results and the interpretation presented herein are consistent with the data and interpretations presented in the other sections of this manuscript—XPS spectrum of the $n = \frac{1}{2}$ hydrino; excess heat from the electrolysis of aqueous potassium carbonate; and mass spectral data for the dihydrino molecule, Sec. V, which follows.

TABLE VIII

Data[9] Near the Predicted $\frac{1}{3} \rightarrow \frac{1}{4}$ Transition*

λ (Å)	Counts	Background	Counts − Background
125.82	26	21.58	4.42
127.10	22	21.32	0.68
128.37	18	19.50	−1.50
129.64	29	20.28	8.72
130.90	18	19.76	−1.76
132.15	20	19.50	0.50
133.41	19	19.50	−0.50
134.65	19	20.80	−1.80

*130.2 Å.

V. IDENTIFICATION OF THE DIHYDRINO MOLECULE

When hydrogen atoms bind to metals, they demonstrate a high degree of mobility, as shown by electron energy loss spectroscopy (EELS) (Ref. 10). A mobile hydrogen atom can bind with a neighboring hydrogen atom to form a diatomic molecule, H_2; this happens routinely in the electrolysis of aqueous solutions. We have shown earlier that the $n = \frac{1}{2}$ hydrino is produced with the release of energy (Sec. II) during the electrolysis of aqueous potassium carbonate and that the $n = \frac{1}{2}$ hydrino is found on the nickel surface (Sec. III). Thus, it is reasonable to predict that dihydrino molecules should be produced from these $n = \frac{1}{2}$ hydrinos.

Specifically, it is known that two hydrogen atoms, $H(n = 1)$, can react to form a diatomic molecule, $H_2(n = 1)$, with a bond energy of 4.75 eV:

$$2H(n = 1; r = a_H) \rightarrow H_2[n = 1; r_e = \sqrt{2}a_H] \quad (24)$$

where r_e is the internuclear distance. Here, we assert that two $n = \frac{1}{2}$ hydrino atoms can similarly react to form a dihydrino molecule[2]:

$$2H\left(n = \frac{1}{2}; r = \frac{a_H}{2}\right) \rightarrow H_2\left[n = \frac{1}{2}; r_e = \frac{\sqrt{2}}{2}a_H\right] . \quad (25)$$

The bond energy for the dihydrino molecule should be much larger than the bond energy for the dihydrogen molecule—certainly more than twice as large.

Furthermore, dihydrogen molecules form dihydrogen molecular ions when they are singly ionized. The ionization energy is 15.46 eV.

$$H_2[n=1; r_e=\sqrt{2}a_H] \rightarrow H_2^+[n=1; r_e=2a_H] + e^- \quad . \tag{26}$$

Similarly, dihydrino molecules should form dihydrino molecular ions when they are singly ionized[2]:

$$H_2\left[n=\frac{1}{2}; r_e=\frac{\sqrt{2}}{2}a_H\right] \rightarrow H_2^+\left[n=\frac{1}{2}; r_e=\frac{2a_H}{2}\right] + e^- \quad . \tag{27}$$

The ionization energy for the dihydrino molecule should be much larger than the ionization energy for the dihydrogen molecule (certainly more than the ionization of the $n = \frac{1}{2}$ hydrino, 54.4 eV).

Thus, we explored the possibility of using mass spectroscopy to discriminate $H_2(n = 1)$ from $H_2(n = \frac{1}{2})$ on the basis of the large difference between the ionization energies of the two species.

V.A. Sample Collection and Preparation

One liter of electrolytic gases was collected from a potassium carbonate electrolysis cell producing excess power (experiment 14 of Ref. 5) in a high-vacuum gas collection bulb. One litre of electrolytic gases from an identical sodium carbonate electrolysis cell that showed no excess heat was collected similarly. These electrolysis gases were cryofiltered according to the method of Bush[11] and collected in two-port 250-ml high-vacuum sample bulbs. A schematic of the cryofiltration apparatus appears in Fig. 13. There were three additional control samples:

1. a sample bulb filled with molecular hydrogen (not cryofiltered)
2. a sample bulb filled with molecular hydrogen which had been cryofiltered
3. for a background comparison, a bulb with gases collected from the cryofilter in the absence of any sample introduction (referred to as cryofiltered alone in the following discussion).

The (predicted) dihydrino molecules were also enriched in the electrolytic gases by partial combustion. About 1650 ml of the electrolysis gases was collected in a mylar balloon from a potassium carbonate electrolysis cell producing excess power (experiment 14 of Ref. 5). The gas was transferred into an elastomer bladder in three aliquots. The bladder contained a wetted spark plug, which was activated after the transfer of each aliquot causing an explosion of the gas contents and combustion of most of the gaseous contents. The volume of the bladder following three combustions was 70 ml. These gases were not cryofiltered and are referred to as postcombustion gases in the following discussion.

V.B. Mass Spectroscopy

The mass spectroscopy was performed by Schrader Analytical and Consulting Laboratories, Inc. using an AEI MS 30 with a VG 7070 source set at a sensitivity

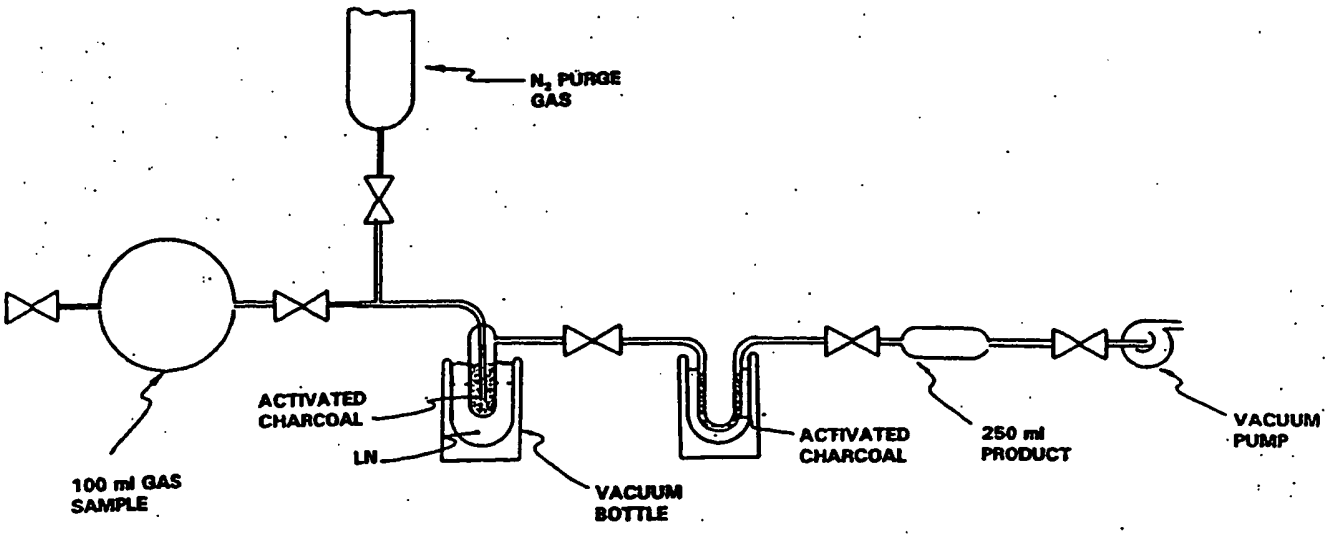

Fig. 13. Schematic of the cryofiltration apparatus.

of 700. The ionization energy was calibrated to within ±1 eV.

Mass spectra of the following (a) cryofiltered gases from potassium carbonate electrolysis cells, (b) cryofiltered gases from sodium carbonate electrolysis cells, (c) uncryofiltered molecular hydrogen, (d) cryofiltered molecular hydrogen, and (e) gases from the cryofilter alone were taken. The intensity of the $m/e = 1$ and $m/e = 2$ peaks was recorded while varying the ionization potential (IP) of the mass spectrometer. The volume of sample gas injected into the mass spectrometer at each IP setting was made identical by evacuating the connection between the sample and the stopcock of the spectrometer, opening the evacuated volume to the sample vessel, closing the sample stopcock, and then opening the stopcock to the spectrometer. The entire range of masses through $m/e = 70$ was measured following the determinations at $m/e = 1$ and $m/e = 2$.

Mass spectra of the postcombustion gases were taken at IP = 70 eV for the entire range of masses through $m/e = 70$. Then, high resolution [0.001 atomic mass unit (AMU)] magnetic sector mass spectroscopy was performed on the postcombustion gas sample and the uncryofiltered molecular hydrogen at a nominal mass to charge ratio of 2 at 25 eV [above the ionization energy of molecular hydrogen yet below the expected ionization energy of $H_2(n = \frac{1}{2})$] and at 70 eV [above the expected ionization energy of $H_2(n = \frac{1}{2})$]. The data were displayed on an oscilloscope (see footnote p on p. 1700). The scan speed and oscilloscope sweep speed were adjusted so that mass differences of 0.001 AMU would give distinctly separate peaks, resolved nearly to baseline. The gas sample pressure was adjusted to provide peaks of essentially the same intensity of ~0.5 V from the baseline to the peak. Photographs of the oscilloscope traces of the $m/e = 2$ ion were made under the following conditions: resolution, 2000; energy, 25 and 70 eV; scan speed, 30 s/decade; scope speed, 5 ms/division; scope voltage setting, 0.2 V/division.

V.C. Results and Discussion

In all samples, the only peaks detected in the mass range $m/e = 3$ to 70 were consistent with trace air contamination (argon, nitrogen, oxygen, water vapor).

The results of the mass spectroscopic analysis ($m/e = 2$) with varying ionization potential of molecular hydrogen and various cryofiltered gases are given in Table IX. For molecular hydrogen, not cryofiltered, there is no signal intensity at IP = 13 eV (less than the ionization energy of H_2, 15.46 eV) and there is a significant signal intensity at 28 eV. Above 28 eV the signal intensity increases (roughly) linearly with IP. In independent experiments, it was determined that the relative signal intensity [for example, the ratio (signal intensity at IP = 79 eV)/(signal intensity at IP = 23 eV)] of molecular hydrogen was independent of mass spectrometer sensitivity and sample pressure. The signal intensity for the uncryofiltered molecular hydrogen was much greater than the signal intensity for all of the cryofiltered samples because, as expected, the number of molecules successfully passing through the cryofilter was quite small. Note, for example, that the cryofilter removes essentially all of the molecular hydrogen (Table IX, H_2 cryofiltered). The cryofilter itself does not release any unusual species with a mass to charge ratio of 2 (Table IX, cryofilter alone).

The greatest signal intensity for any of the cryofiltered samples occurs with the gases from the K_2CO_3 cell at IP = 79 eV. There is also a slightly elevated signal with the gases from the Na_2CO_3 cell at IP = 79 eV. Both of these samples had a significant $m/e = 18$ water peak. The base peak for water vapor is at $m/e = 18$, but water vapor also gives peaks at $m/e = 1$ and $m/e = 2$. Independent experiments show that the ratio (at 79 eV) (signal intensity $m/e = 1$)/(signal intensity $m/e = 2$) is 6 for water vapor. The data in Table X show that the ratio of the signal intensities (at 79 eV), $m/e = 1$ to $m/e = 2$, is 0.150/0.025 or 6.0 for the gases from the

TABLE IX

Mass Spectroscopic Analysis of Molecular Hydrogen and Cryofiltered Samples with Varying Ionization Potential at $m/e = 2$

Ionization Potential (eV)	Intensity of Signal				
	H_2 Not Cryofiltered	H_2 Cryofiltered	Gases from Cryofilter Alone	Gases from Na_2CO_3 Cell	Gases from K_2CO_3 Cell
13	0.0	0.000	0	0.000	0.000
23	2.5	0.000	0	0.004	0.025
45	5.4	0.005	0	0.000	0.020
79	6.8	0.005	0	0.025	0.24

Na_2CO_3 cell. Thus, the signal intensity at $m/e = 1$ and $m/e = 2$ (IP = 79) with the Na_2CO_3 gases is from residual water vapor in the vacuum system. Note, however, that this ratio for the gases from the K_2CO_3 cell is 0.060/0.24 or 0.25—much too low to be from water vapor. Assuming that all of the signal intensity at $m/e = 1$ is from water vapor, the contribution of water vapor to the $m/e = 2$ peak should be 0.060/6 or 0.01—negligible in comparison to the observed signal of 0.24. Thus, the large increase in signal intensity at $m/e = 2$ between IP = 45 eV and IP = 79 (0.020 to 0.24, a factor of 12) for cryofiltered gases from the potassium carbonate electrolysis does not appear to be caused by molecular hydrogen or water vapor. A species with a much higher ionization potential than molecular hydrogen, somewhere between 45 to 79 eV, is present. Systematic scans while varying the IP show that the onset of the ionization of this species is at 63 eV.

Photographs of the high resolution magnetic sector mass spectra of the uncryofiltered molecular hydrogen sample ($m/e = 2$) at 25 eV and at 70 eV are given in Fig. 14. Both peaks have a typical shape. Photographs of the high resolution magnetic sector mass spectra of the postcombustion gases ($m/e = 2$) at 25 eV and 70 eV are given in Fig. 15. Notice that there is *one* peak at 25 eV and that this peak has a typical shape. However, there are *two* peaks at 70 eV. Only a limited number of "traditional" $m/e = 2$ peaks are possible—H_2^+, D^+, He^{2+}—and only one of these could cause a peak at $m/e = 2$ in these samples:

1. $H_2^+(n = 1)$ causes one of the peaks.
2. Deuterium D^+ is eliminated because (a) light water, not heavy water, was used and (b) no HD^+(g), $m/e = 3$, peak was observed.
3. He^{2+} was eliminated because no He^+, $m/e = 4$, peak was observed.

Thus, some other species is causing the second peak at 70 eV. It is likely that $H_2^+(n = \frac{1}{2})$ would be ionized at 70 eV and that it would not be ionized at 25 eV, but the mass of $H_2^+(n = \frac{1}{2})$ would only be ~100 eV (or 1×10^{-7} AMU) less than $H_2^+(n = 1)$—not distinguishable on the basis of mass even with high resolution mass spectroscopy. We note, however, that the magnetic moment of the $H_2^+(n = \frac{1}{2})$ ion has been predicted to have a larger magnetic moment than the $H_2^+(n = 1)$ ion.[2] It is likely, then, that the two molecules would have different flights in the magnetic sector (MS). We assert, therefore, that the partial combustion of the evolved gases from the electrolysis of aqueous K_2CO_3 yields unreacted, molecular hydrogen molecules *and* unreacted, dihydrino molecules. In the mass spectrum, the $H_2^+(n = 1)$ peak is present at 25 eV and at 70 eV. The harder-to-ionize dihydrino molecule, however, is *not* present at 25 eV and $H_2^+(n = \frac{1}{2})$ appears only at the higher IP, 70 eV. The possibility of artifact was ruled out by studying normal hydrogen over a range of pressures and ionization energies. No double peaks ($m/e = 2$) were observed.

TABLE X

Mass Spectroscopic Analysis of Cryofiltered Gases from Na_2CO_3 and K_2CO_3 Cells with Varying Ionization Potential at $m/e = 1$ and 2

Ionization Potential (eV)	Intensity of Signal			
	Gases from Na_2CO_3 Cell at Mass to Charge Ratio (m/e)		Gases from K_2CO_3 Cell at Mass to Charge Ratio (m/e)	
	1	2	1	2
13	0.000	0.000	0.000	0.000
23	0.014	0.004	0.010	0.025
45	0.040	0.000	0.024	0.020
79	0.150	0.025	0.060	0.24

We conclude that hydrinos are produced on or near the cathode surface as hydrogen atoms are stimulated to relax to quantized potential energy levels below that of the "ground state" (see Sec. II.E) and that two hydrinos, $H(n = \frac{1}{2})$, react to form the lower energy dihydrino molecule.

V.D. Alternative Explanations of Related Experiments by Other Researchers

The internuclear distance of the dihydrino molecule is a factor of 2 shorter than the internuclear distance of the normal hydrogen molecule.[2] The same ratio applies when deuterium nuclei replace the protons. In accordance with the predictions of Fukai[12] relating fusion reaction rates to internuclear separation, production of the dideutrino molecule (hydrino molecule with the protons replaced by deuterons) could account for the observation of detectable levels of tritium over long duration electrolysis experiments.[1,13,14]

We have reported previously our interpretation[5] that Miles[11,15-17] observed the dideutrino molecule as a species with a mass to charge ratio of four and having a higher ionization potential than normal molecular deuterium. Miles was using mass spectroscopy to analyze the cryofiltered gases evolved from excess power producing electrolysis cells (palladium cathode and a $LiOD/D_2O$ electrolyte; a catalytic couple of 27.54 eV). And, we have previously reported our interpretation[5] that Yamaguchi[18,19] observed the dideutrino molecule as a large shoulder on the D_2 peak and a split D_2 peak during the high resolution (0.001 AMU) quadrupole mass spectroscopic analysis of the gases released from

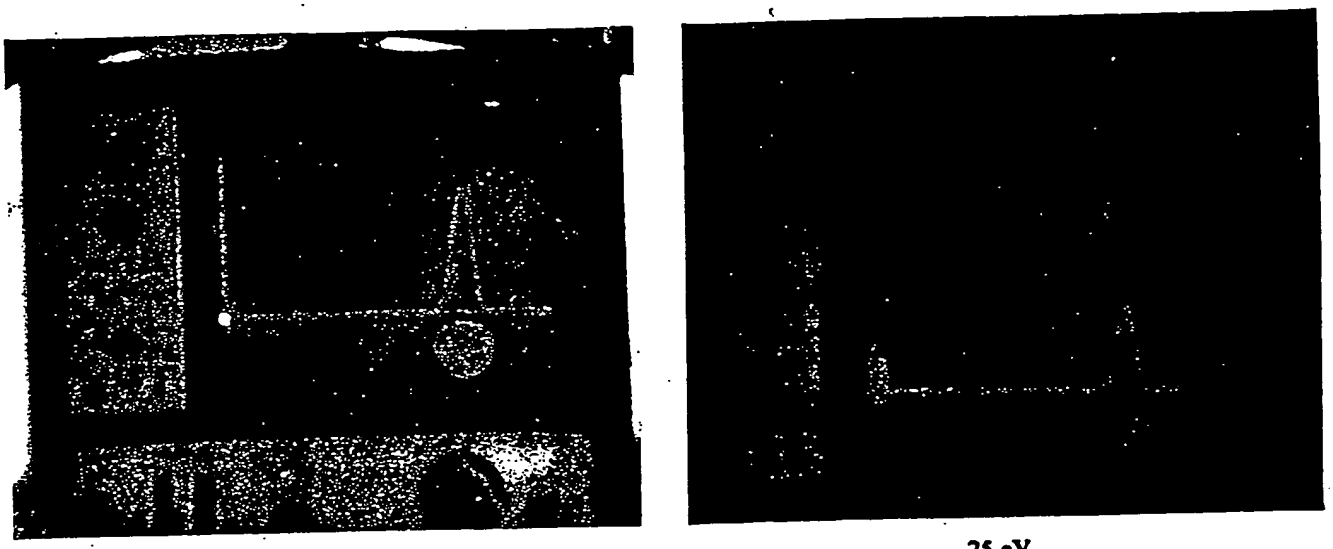

70 eV 25 eV

Fig. 14. The high resolution magnetic sector mass spectra at $m/e = 2$ of molecular hydrogen at 25 and 70 eV. Only one peak is found: $H_2(n = 1)$ ionization.

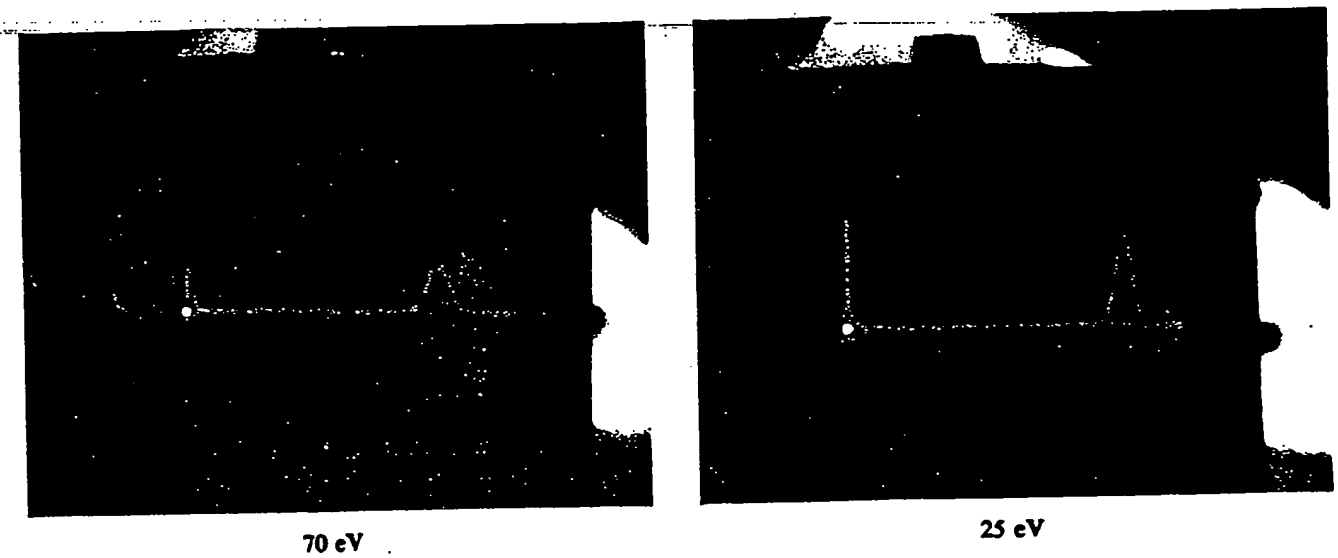

70 eV 25 eV

Fig. 15. The high resolution magnetic sector mass spectra at $m/e = 2$ of the postcombustion gases at 25 and 70 eV. Two peaks are found at the higher IP: $H_2(n = 1)$ ionization and $H_2(n = \frac{1}{2})$ ionization. The two peaks were about of the same intensity in this sample. In other (similarly prepared) samples, however, the two peaks had different intensities.

excess heat producing, deuterium-loaded, oxide-coated palladium sheets (a catalytic couple of 27.2 eV).

VI. SUMMARY

The complete theory which predicts fractional quantum energy levels of hydrogen and the exothermic reaction whereby lower-energy hydrogen is produced is given elsewhere.[1,2]

Excess power and heat were observed during the electrolysis of aqueous potassium carbonate. Flow calorimetry of pulsed current electrolysis of aqueous potassium carbonate at a nickel cathode was performed in a single-cell dewar. The average power out of 24.6 W exceeded the average input power (voltage times current) of 4.73 W by a factor >5. The total input energy (integration of voltage times current) over the entire duration of the experiment was 5.72 MJ; whereas, the total output energy was 29.8 MJ. No excess heat was

observed when the electrolyte was changed from potassium carbonate to sodium carbonate. The source of heat is assigned to the electrocatalytic, exothermic reaction whereby the electrons of hydrogen atoms are induced to undergo transitions to quantized energy levels below the conventional "ground state." These lower energy states correspond to fractional quantum numbers: $n = \frac{1}{2}, \frac{1}{3}, \frac{1}{4}, \ldots$. Transitions to these lower energy states are stimulated in the presence of pairs of potassium ions (K^+/K^+ electrocatalytic couple) which provide 27.2-eV energy sinks.

We report the identification of the $n = \frac{1}{2}$ hydrogen atom, $H(n = \frac{1}{2})$. Samples of the nickel cathodes of aqueous potassium carbonate electrolytic cells and aqueous sodium carbonate electrolytic cells were analyzed by XPS. A broad peak centered at 54.6 eV was present only in the cases of the potassium carbonate cells. The binding energy (in vacuum) of $H(n = \frac{1}{2})$ is 54.4 eV. Thus, the theoretical and measured binding energies for $H(n = \frac{1}{2})$ are in excellent agreement.

Further experimental identification of hydrinos—down to $H(n = \frac{1}{5})$—can be found in our alternative explanation for the soft X-ray emissions of the dark interstellar medium observed by Labov and Bowyer. We believe that the agreement between the experimental spectrum and the energy values predicted for the proposed transitions is remarkable.

We have identified the reaction product of two $H(n = \frac{1}{2})$ atoms, the dihydrino molecule, by mass spectroscopy. The mass spectrum of the cryofiltered gases evolved during the electrolysis of a light water K_2CO_3 electrolyte with a nickel cathode demonstrated that the dihydrino molecule, $H_2(n = \frac{1}{2})$, has a higher ionization energy, about 63 eV, than normal molecular hydrogen, $H_2(n = 1)$, 15.46 eV. The high resolution (0.001 AMU) magnetic sector mass spectroscopic analysis of the postcombustion gases indicated the presence of two peaks of nominal mass, two at 70 eV, and one peak at 25 eV. The same analysis of molecular hydrogen indicates only one peak at 25 eV and one peak at 70 eV. In the case of the postcombustion sample at 70 eV, one peak was assigned as the hydrogen molecular ion peak, $H_2^+(n = 1)$, and one peak was assigned as the dihydrino molecular peak, $H_2^+(n = \frac{1}{2})$.

Based on our analysis[5] of the raw data of Miles[11,15-17] and Yamaguchi,[18,19] we interpret their results as evidence of the dideutrino, $D_2(n = \frac{1}{2})$; heavy hydrogen, ^2H, was used in their experiments, not ^1H.

ACKNOWLEDGMENTS

Special thanks to the following: G. Simmons and A. Miller of Lehigh University who performed the XPS analysis; J. DeFever of Schrader Analytical and Consulting Laboratories, Inc., who performed the mass spectroscopy; S. LaBov and S. Bowyer for providing spectral data; J. Farrell, Department of Chemistry, Franklin & Marshall College, for assistance in preparing this manuscript; D. Backman, Department of Physics and Astronomy, Franklin & Marshall College, for his many suggestions and, in particular, for his help in deriving the transition probability from the Labov and Bowyer data.

REFERENCES

1. R. MILLS, *Unification of Spacetime, the Forces, Matter, and Energy*, Technomics Publishing Company, Lancaster, Pennsylvania (1992).

2. R. MILLS, "Energy/Matter Conversion Methods and Structures," U.S. Patent Application (Aug. 16, 1993).

3. H. A. HAUS, *Am. J. Phys.*, 54, 1126 (1986).

4. R. L. MILLS and S. P. KNEIZYS, "Excess Heat Production by the Electrolysis of an Aqueous Potassium Carbonate Electrolyte and the Implications for Cold Fusion," *Fusion Technol.*, 20, 65 (1991).

5. R. MILLS, W. GOOD, and R. SHAUBACH, "Dihydrino Molecule Identification," *Fusion Technol.*, 25, 103 (1994).

6. V. NONINSKI, "Excess Heat During the Electrolysis of a Light Water Solution of K_2CO_3 with a Nickel Cathode," *Fusion Technol.*, 21, 163 (1992).

7. R. NOTOYA and M. ENYO, *Proc. 3rd Annual Conf. Cold Fusion*, Nagoya, Japan, October 21-25, 1992, p. 421, H. IKEGAMI, Ed., Universal Academy Press, Inc., Tokyo (1992).

8. S. BOWYER, G. FIELD, and J. MACK, *Nature*, 217, 32 (1968).

9. S. LABOV and S. BOWYER, *Ap. J.*, 371, 810 (1991).

10. R. NIEMINEN, *Nature*, 365, 289 (1992).

11. B. F. BUSH, J. J. LAGOWSKI, M. H. MILES, and G. S. OSTROM, *J. Electroanal. Chem.*, 304, 271 (1991).

12. Y. FUKAI, "The ABC's of the Hydrogen-Metal System," *Proc. 3rd Annual Conf. Cold Fusion*, Nagoya, Japan, October 21-25, 1992, p. 265, H. IKEGAMI, Ed., Universal Academy Press, Inc., Tokyo (1992).

13. M. FLEISCHMANN, S. PONS, W. ANDERSON, L. JUN LI, and M. HAWKINGS, *J. Electroanal. Chem.*, 287, 293 (1990).

14. E. STORMS and C. TALCOTT, "Electrolytic Tritium Production," *Fusion Technol.*, 17, 680 (1990).

15. M. H. MILES, B. F. BUSH, G. S. OSTROM, and J. J. LAGOWSKI, *The Science of Cold Fusion: Proc. 2nd Annual Conf. Cold Fusion*, Como, Italy, June 29-July 4, 1991, T. BRESSANI, E. DEL GIUDICE, and G. PREPARATA,

Eds., Vol. 33, p. 363, in *Conf. Proc. Italian Physical Society*, Bologna (1992).

16. M. H. MILES, R. A. HOLLINS, B. F. BUSH, J. J. LAGOWSKI, and R. E. J. MILES, *J. Electroanal. Chem.*, 346, 99 (1993).

17. M. H. MILES and B. F. BUSH, *Proc. 3rd Annual Conf. Cold Fusion*, Nagoya, Japan, October 21-25, 1992, p. 189, H. IKEGAMI, Ed., Universal Academy Press, Inc., Tokyo (1992).

18. E. YAMAGUCHI and T. NISHIOKA, "Direct Evidence for Nuclear Fusion Reactions in Deuterated Palladium," *Proc. 3rd Annual Conf. Cold Fusion*, Nagoya, Japan, October 21-25, 1992, p. 179, H. IKEGAMI, Ed., Universal Academy Press, Inc., Tokyo (1992).

19. E. YAMAGUCHI and T. NISHIOKA, Personal Communication regarding helium-4 production from deuterated palladium at low energies, Nipon Telegraph & Telephone Basic Research Laboratories (1992).

Randell L. Mills (BA, chemistry, Franklin and Marshall College, 1982; MD, Harvard University, 1986) developed magnetic susceptibility imaging for high-resolution internal vascular images, the MIRAGE cancer therapy, and the Luminide drug delivery molecule. He is founder of Mills Technology, HydroCatalysis Power Corporation, and Luminide Pharmaceutical Corporation.

William R. Good (BS, chemistry, Franklin and Marshall College) has been studying hydrogen emission by catalytic thermal electronic relaxation. He is currently research director at HydroCatalysis Power Corporation.